The Wettability of Ceramic-Coated Steel Substrates by Liquid Metals

Musbah Mahfoud
Mining and Metallurgical Engineering
McGill University

A thesis submitted to the Faculty of Graduate Studies
and research in partial fulfilment of the requirements for
the Degree of Masters of Engineering

ABSTRACT

Hazelett Caster steel belts, used to continuously cast strips and slabs by the twin-belt caster, are often coated with a thermally-sprayed ceramic powder. One of the major advantages of the coating is to reduce wettability between the molten metal and the moving steel belt, thereby, minimizing friction between the belt and cast, and allowing easy stripping of the strand.

In this research, the sessile drop method was used to study the wettability of pure tin and aluminum alloys 3003 and 3105 on four plasma-coated ceramic substrates ($MgO.ZrO_2$, ZrO_2, Al_2O_3, and, TiO_2). Uncoated steel and copper substrates were also investigated. The wettability of tin on all substrates was investigated at 300°C and 690°C, whereas that of the aluminum alloys was investigated at 690°C only.

It was found that the wettability of liquid metals on coated substrates was less than that on uncoated substrates. In addition, metal drops which solidified on the uncoated substrates showed a strong adherence at the interface, whereas drops solidified on the coated substrates showed no adherence, and were easily removed from the substrates.

Among the four coated substrates investigated in this work, magnesium zirconate ($MgO.ZrO_2$) showed the least wettability, while titania (TiO_2) showed the most wettability. Alumina (Al_2O_3) and zirconia (ZrO_2) exhibited intermediate wettability between those of magnesium zirconate and titania.

RÉSUMÉ

Les courroies en acier de la Roulette Hazelett, utilisées par les roulettes à courroies jumelles pour la coulée continue de feuillards et de brames d'acier, sont souvent recouverts d'une couche de poudre de céramique pulvérisée à haute température. Un des avantages principals de cette couche est de réduire la mouillabilité entre le métal liquide et la courroie d'acier en mouvement. Ceci minimise la friction entre la courroie et le moulage et permet de décoller le moulage facilement.

Dans le cadre de cette étude, le procédé de la goutte sessile a été utilisée pour étudier la mouillabilité de l'étain pur et des alliages d'aluminium 3003 et 3105 sur quatre substrats de céramique appliqués par plasma ($MgO.ZrO_2$, ZrO_2, Al_2O_3, and TiO_2). Des substrats d'acier et de cuivre non recouverts ont aussi été étudiés. La mouillabilité de l'étain sur tous les substrats a été étudiée à 300°C et 690°C. Celle des alliages d'aluminium a été testée uniquement à 690°C.

L'étude a démontré que la mouillabilité des métaux liquides sur les substrats recouverts était plus faible que sur les substrats non recouverts. De plus, les gouttes de métal qui se sont solidifiées sur les substrats non recouverts adhéraient fortement à l'interface. Celles solidifiées sur des substrats recouverts ne démontraient aucune adhérence et ont été enlevées facilement.

Parmi les quatre substrats recouvert étudiés dans le cadre de ce projet, le zirconate de magnésium ($MgO.ZrO_2$) avait la mouillabilité la plus faible tandis que le dioxyde de titane (TiO_2) avait la mouillabilité la plus élevée. L'oxyde d'aluminium (Al_2O_3) et la zircone (ZrO_2) avaient des mouillabilités intermédiaires, entre celles du zirconate de magnésium et du dioxyde de titane.

Acknowledgement

I would like to express my utmost appreciation to my thesis supervisor Dr. R. I. L. Guthrie for his continuous encouragement and illuminating guidance throughout the course of this work.

I would also like to express my sincerest appreciation to Mr. Wojtec Szczypiorski and Mr. Jerry Allyn, from the Hazelett Strip Casting Corporation, for supplying most of the test samples, and, for their valuable instructions that made this work possible.

I'm thankful to Dr. D. Doutré, from Alcan International in Kingston, Ontario, for supplying the aluminum samples.

I wish to thank Prof. J. Toguri of the Department of Metallurgy and Material Science, at the University of Toronto, for letting me use his laboratory facilities.

Very special thanks go to Prof. J. E. Gruzleski for his assistance with identifying the microstructures of the solidified samples, and Mrs Helen Campbell for her assistance in the SEM analyses.

Finally, I'm very grateful to my fellow students, in the Department of Mining and Metallurgical Engineering, for their helpful suggestions and valuable discussions that contributed significantly to this thesis. Their contributions are readily acknowledged.

TABLE OF CONTENTS

LIST OF FIGURES

LIST OF TABLES

CHAPTER
ONE

INTRODUCTION

1.1 THE PROBLEM

During continuous casting of metals, problems such as cold shuts and/or surface cracking may result in the final product, because of early solidification in the meniscus region due to non-uniform heat transfer through the mould. The non-uniformity of heat transfer may also result in mould distortion affecting the quality of the cast product.

1.1.1 Metal Delivery and Meniscus Freezing

Metal delivery remains a key factor in the commercialisation of strip and slab casting technology. Surface and internal quality of the cast material require metal delivery systems which achieve meniscus stability and uniform shell growth.

The stability of the meniscus, which defines the first point of contact between the liquid metal and the substrate, Figure (1.1), is fundamental to the resulting surface quality[1]. The conditions at the meniscus affect the interfacial heat transfer, which determines the initial solidification structure[2]. Thus, events which take place during the first fraction of a second of melt/substrate interaction can set the framework for the development of final cast properties.

During casting with moving moulds (e.g., belts or wheels) the melt is subjected to displacements relative to the moving mould. These displacements are not steady because of variability in liquid metal feed rates. Thus, intermittent movements can occur and, for a short period, the meniscus formed against the mould wall can be kept static, or, at least be restricted to a very low displacement, relative to the mould. During this short period solidification can take place to a larger extent than when a steady, fast melt displacement occurs along the mould-wall surface[3].

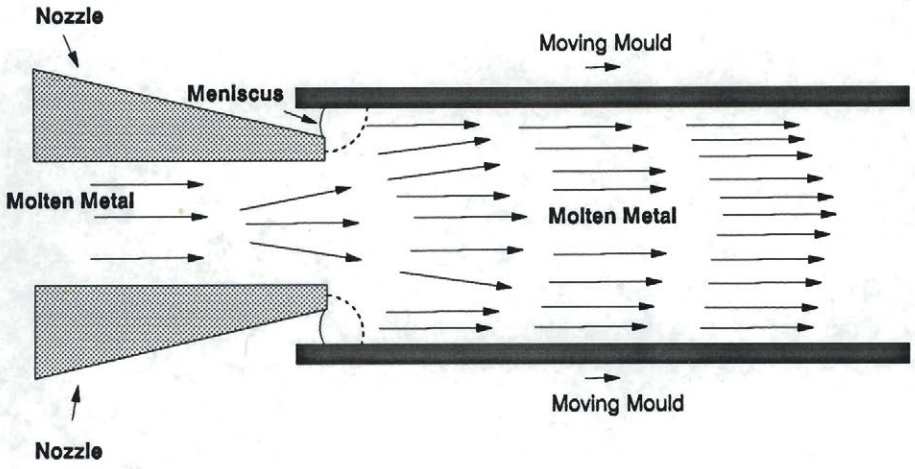

Figure (1.1) Meniscus Formation

Solidification theory indicates that no solidification will take place in the melt until the superheat has been dissipated. However, the strong chilling provided by the mould can produce a steep temperature gradient, so some solid may be formed at an early stage. Much evidence suggests that a significant solid shell can form in only fractions of a second[4].
Therefore, the critical area of continuous casting system (especially the horizontal type) is the meniscus region.

By careful selection of key parameters the stability and non-freezing requirements can be satisfied to achieve a reliable feeding system.

The factors that can cause instability of the meniscus , along with features that promote meniscus stability, are shown in Table (1.1).

Table (1.1) Factors affecting meniscus stability[5].

MENISCUS CONTROL	
INSTABILITY	STABILITY
• Partial Freezing	• Fluid flow to meniscus area
• Irregular position and movement	• Constrained liquid pool under positive pressure
• Reoxidation	• Enclosed delivery system
• Non-uniform substrate condition	• Controlled melt/ substrate interaction

The last factor in Table (1.1) indicates that the substrate, i.e.,casting mould, plays a major roll in controlling the heat transfer, and subsequently the partial solidification of the meniscus region.

1.2 THE CONTINUOUS CASTING MOULD

A continuous casting mould, used to continuously cast a slab or strip, is a complicated reactor, which performs several different functions under extreme conditions. It is:

- a heat exchanger that handles very high heat flux densities,
- a solidification device that builds up a thin solid shell made of a fragile material,

- and a die which gives its shape to the strip, slab, or a billet without tearing the brittle shell. Product quality comes about if and only if each of these functions is performed homogeneously in space and time and doing so requires a wealth of care and subtlety in process metallurgy[6].

Within the entire context of continuous casting, the mould must be regarded as the heart of the operation. The efficiency of heat extraction in the mould is ultimately responsible for surface quality of the cast product and the productivity of the casting machine. In addition to the defects that can result from meniscus freezing, excessive and/or uneven heat removal from the strand will also result in thermally induced stresses that may ultimately cause longitudinal cracks in the newly solidified shell[7].

Evolution of continuous casting, that can lead to a defect free near-net shape cast product, will depend critically on the performance of the mould where surface (and sub-surface) quality is made and many production problems begin. The mould of continuous casting is the matrix in which the surface of the final product is produced.

Although good progress has been made to solve some of the problems associated with continuous casting, mould distortion and surface defects are still a major problem. To eliminate these casting problems, the continuous casting mould must be made of a material that can efficiently control the heat transfer during solidification and allow easy stripping of the cast product.

1.3 MOULD COATING

While the concept of foundry coatings has been known for quite a long time, only recently that the idea of coating of a continuous casting mould has been given special attention.

Today, the ever increasing demand for mould coating to enhance casting quality and cope with more stringent specifications, especially in the area of reduced cast metal section thickness, necessitates more research to be done to find a suitable coating for most of the casting operations. The ability to incorporate a certain type of a ceramic material with the exclusive application characteristics of the coating would certainly solve most of today's casting problems.

The demands for mould coatings with properties to cope with high levels of productivity, tighter specifications and dimensional accuracy and high rate repetitive casting, with the resultant commercial advantages, have resulted in the development of specific coatings and application methods to suit the casting requirements and environments. In general, a suitable mould coating is required for several important reasons[8];

(i) mould coating can be used to promote directional solidification,

(ii) a mould coating serves as a lubricant that will prevent sticking of the casting to the mould, provide a smooth surface, and assist in controlling solidification (i.e controlling the heat flow from the metal to the mould) so that sound castings are obtained,

(iii) a coating insulates the poured metal from the chilling effects of the metal mould so that the mould can fill completely,

(iv) a coating isolates the poured metal from the surface of the mould, greatly reducing its erosion, and consequently reducing the development of tiny cracks, and other damages to the mould.

The Hazelett Corporation in Colchester, Vermont, U.S.A, has recently adapted the concept of mould coating by applying a ceramic-based coating to the steel belt used in the twin-belt caster machine. The coating is applied to the belt by flame or plasma spray methods. Results from early trials[8] have shown that a ceramic coating, to the steel belt, can:

a) prolong the surface life of the belt,

b) act as a non-wetting surface, thus lessening the friction between metal and mould,

c) act as a heat transfer moderator, therefore preventing early solidification of molten metal.

1.4 The Aims of this Work

This thesis deals with metal/substrate interaction in the form of a wettability study. The investigation was conducted to study the wettability of pure tin, and aluminum alloys (Al 3003, and Al 3105) on various ceramic coatings used to coat a steel belt. The belt is used as the casting mould in the twin-belt caster. Uncoated substrates of steel and copper were also considered.

The main aims are as follows:

1) To determine the effect of surface coating on wettability.

2) To determine the difference in wettability among the various ceramic coatings investigated in this work.

CHAPTER
TWO

LITERATURE REVIEW

2.1 INTRODUCTION

The concept of producing a final product directly from molten metal began as early as 1857 when Sir Henry Bessemer proposed to produce steel strips between two revolving rolls as shown in Figure (2.1)[10]. By 1921, 0.06″-thick lead strip was being cast and continuously fed to a punch press for making battery grids using this technique[11]. In the late 1930's a number of U.S. and other companies attempted casting aluminum, copper, brass and steel by the two-roll process. Unfortunately, alloys were found to segregate when squeezed close to their freezing points. Also, a backward folding action took place which produced a leafy effect inside the strip[11]. Since then, continuous casting has been undergoing intensive studies in order to achieve a better casting quality in the most economical way.

Despite the fact that there has been no shortage of research on the continuous casting process , the concept of applying a ceramic coating to the continuous casting mould has not received much attention. Nonetheless, it can be helpful in alleviating many problems associated with continuous casting operations.

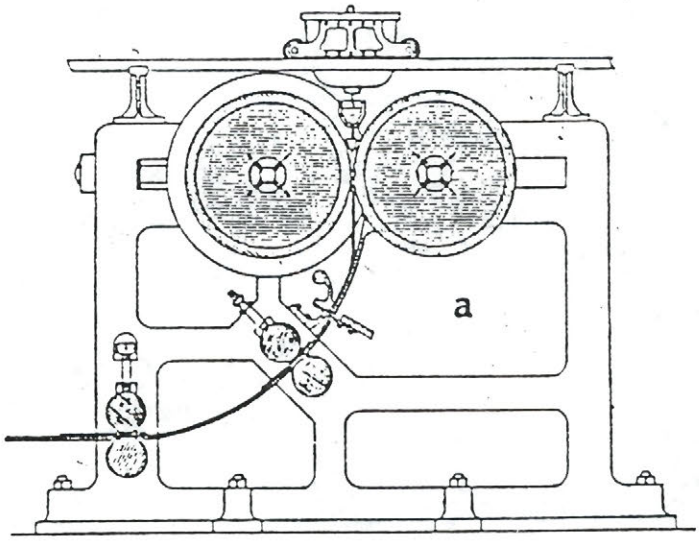

Figure (2.1) The Bessemer Machine[10].

2.2 TYPES OF CONTINUOUS CASTING DEVICES

Past research has led to the development of a number of continuous casting devices. In particular, the field of near-net shape casting has been undergoing an intensive research for over ten years. Six types of heat-extraction devices for casting near-net shapes have been under study. These devices are the single roll, twin roll, twin belt, wheel-belt, single belt and the convex mould. Examples of these devices are given in Figure (2.2)[12].

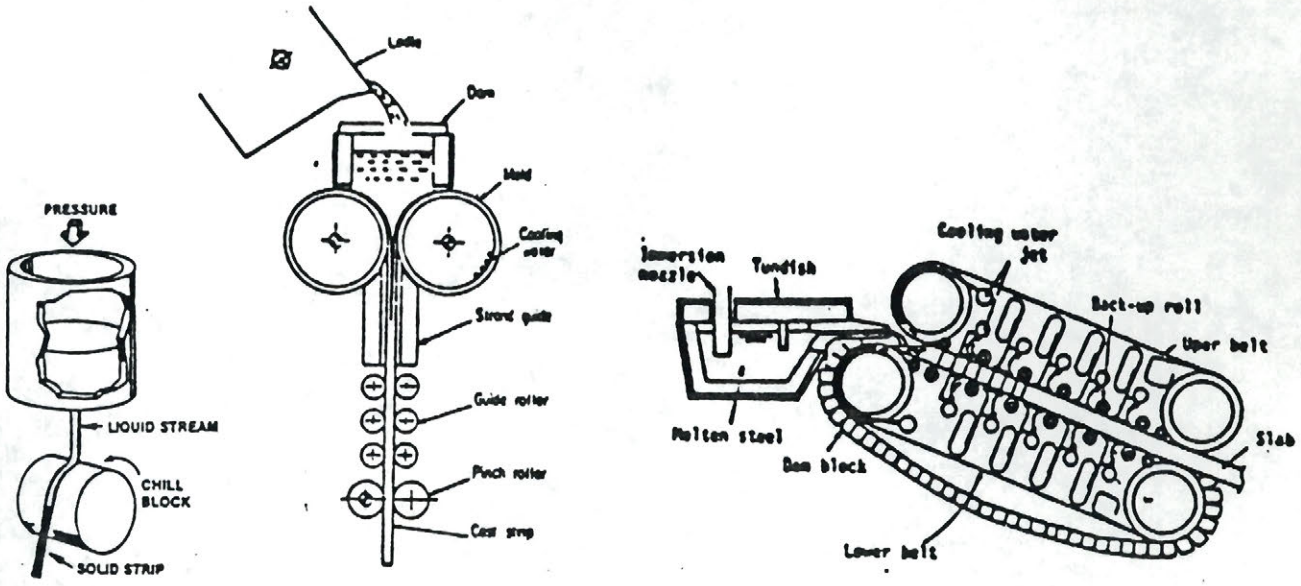

(a) Single Roll (b) Twin Roll (c) Twin Belt

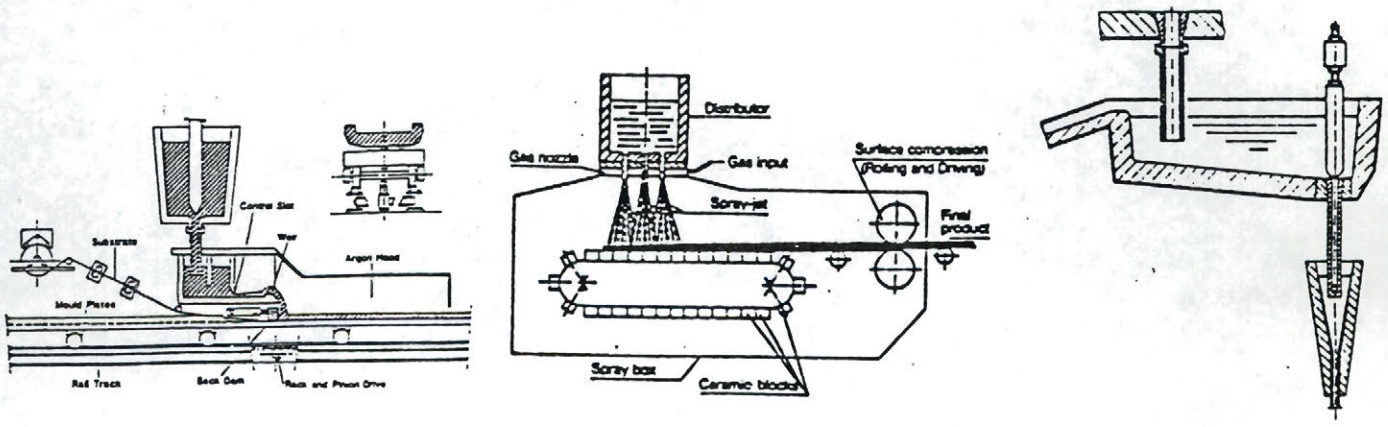

(d) Wheel Belt (e) Single Belt (f) Convex Mould

Figure (2.2) Types of Heat Extraction Devices[12].

With the exception of the twin-roll and the twin belt, all heat- extraction devices are not coated. Thus sticking, excessive friction and resulting surface quality problems, are a major concern in the near-net shape continuous casting process[13].

Nippon Steel uses a nickel-coated copper mould to cast steel on a twin-roll caster[14], whereas the Hazelett Corporation has adapted the use of a ceramic-coated steel belt to cast ferrous and non-ferrous metals on a twin-belt caster.

Since this work was intended to study the wetting aspect of metals on the ceramic-coated mould used in the twin-belt caster, only work on this type of caster was considered. Emphasis was placed on the casting mould (belt), the wetting phenomenon, and the concept of mould coating.

2.3 THE HAZELETT TWIN-BELT CASTER

The Hazelett twin-belt caster, a high production alternative to the twin-roll caster, is manufactured by The Hazelett Strip-Casting Corporation located in Colchester, Vermont, U.S.A. The corporation has been designing and manufacturing continuous casting machines since 1919. In the late 1940's, Hazelett dedicated its efforts to the development of the twin-belt caster design and is now believed to be the world's only commercial supplier of the twin-belt process[15].

Over the last thirty-five years, approximately 70 twin-belt casters have been installed to cast both ferrous and non-ferrous metals. The last statistics indicate that there are, currently, over 50 machines operating in nineteen different countries[15].

The caster produces aluminum alloys such as 1100, 3003, 3105, 5050, and others in widths ranging from 10-60", and casting thicknesses from 2.1" down to 0.6" [16]. The caster also casts aluminum, zinc, copper, lead, and steel in bar and slab widths up to 60" [17]. Strips of zinc, copper, and lead are also cast in thicknesses ranging from 0.39-0.63", 0.59-1.57, 0.51-0.67", respectively[15]. Steel strip is cast in a thickness of about 0.79" [13].

2.3.1 Features of The Twin-Belt Caster

The Hazelett Caster offers a superior dimensional tolerance and surface than conventional casting techniques. The special features of the Hazelett twin-belt continuous casting process include[18]:

- A high solidification rate combined with a four-sided moving mould gives desirable surface characteristics and high production rates.
- Mechanical properties are uniform across the cast width.
- Automatic feeding; only one to two operators required.
- Low operating costs.
- High output - thin strip or billet can be produced with substantially lower capital costs than conventional casting and rolling facilities.

2.3.2 The Twin-Belt System

The Twin-belt system, shown in Figure (2.3), employs a top and a bottom carriage. The top carriage is hydraulically raised to permit mould maintenance. Each carriage has a belt wrapped around grooved pulleys, which simultaneously transport and guide the belt and provide longitudinal tension. Each side of the belt is contained by a chain of steel blocks which are

pinned to an endless stainless steel strip. The thickness of the cast section is governed by interchangeable carriage spacers and can be changed from 3/8″ to 3″, as required[19]. The cast section width is controlled by the spacing of metallic side dam blocks which are carried on steel straps and move with the casting belts. The caster may be operated at any angle between 6° and 20°. Normally, lead, aluminum and zinc are cast at an angle of 6° to 9°, and copper and steel are cast at about 15° [20].

Almost all of the twin-belt installations employ one or more stands of in-line hot rolling consisting of pinch rolls, located at the mould exit and operated at a speed slightly lower than the caster, which compensates for the shrinkage during cooling thus preventing any tension stresses on the slab or strip. The pinch rolls also isolate the mould from down stream effects, such as shearing and rolling vibrations[16].

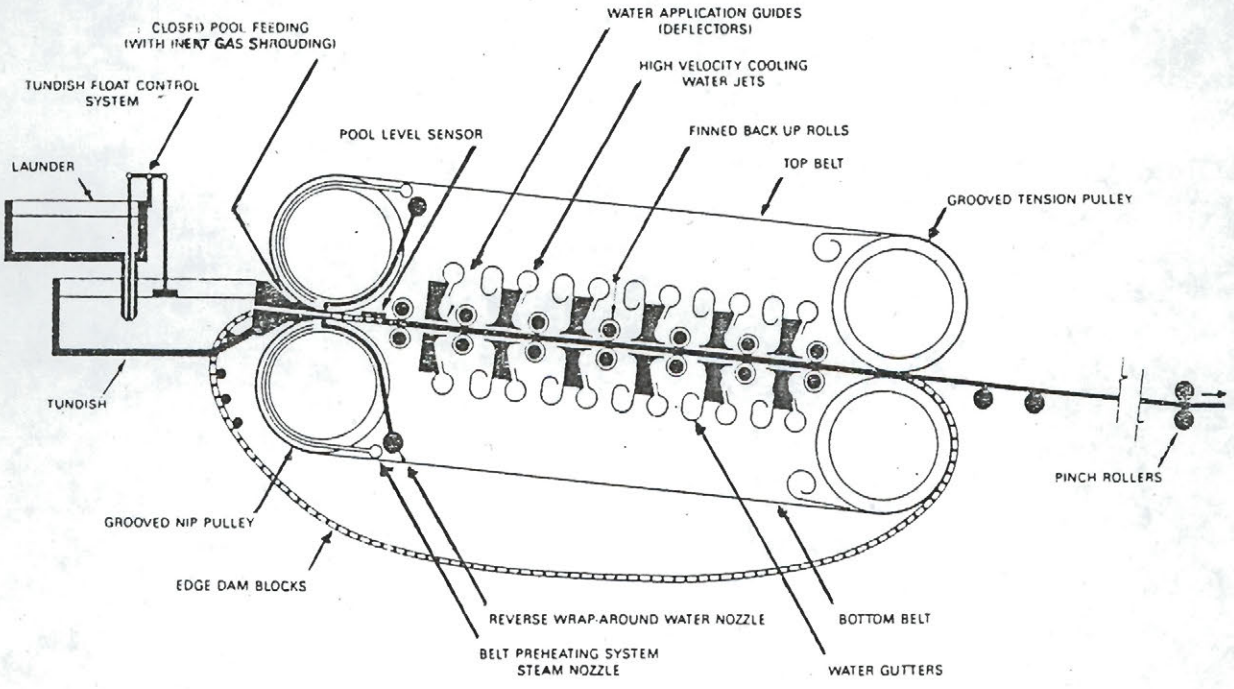

Figure (2.3) The Twin-Belt Casting System[19].

2.3.2.1 The Hazelett Mould

The Hazelett Corporation has investigated a variety of materials for the belts, including the common non-ferrous alloys, copper, titanium, invar, and stainless steel. To date, low carbon, cold rolled steel strip with certain manufacturing variations for each application offers the best combination of physical properties. The steel strip is used in thicknesses between 0.042″ and 0.054″ [21].

The mould length normally used for aluminum slab casting is 70″, measured from the metal entry position to the last back-up roll. However this length may be increased to 101″ or 146″ to provide corresponding increases in production. Mould (belt) width is equal to the maximum desired cast width plus 11″ to cover dam block chains at side seal[17]. The casting surface is roughened by grit blasting, and the belt is then roller levelled on a flatness of less than 0.002″ deviation from a standard straight edge[16].

2.4 PROCESS IMPROVEMENTS ON THE TWIN-BELT CASTER

Between 1975 and the present date, several important improvements have been added to the machine to make it an effective metallurgical process for the production of a variety of alloys. These improvements included; a) metal delivery, b) improved synchronization of caster and pinch rolls, c) belt preheating and, d) belt coating[17].

Since this work deals with metal delivery and mould coating, only points a,c,d will be reviewed.

2.4.1 Atmosphere Shrouded Metal Entry.

In early trials of metal casting using the twin-belt caster, an open pool system was used. Problems such as metal reoxidation, and meniscus instability were encountered. To reduce reoxidation and achieve a better meniscus stability, the closed-pool feeding system, as shown in Figure (2.4), was adapted. In this method, a replaceable high-temperature material nosepiece with parallel passages conveys the molten metal from the tundish into the casting cavity.

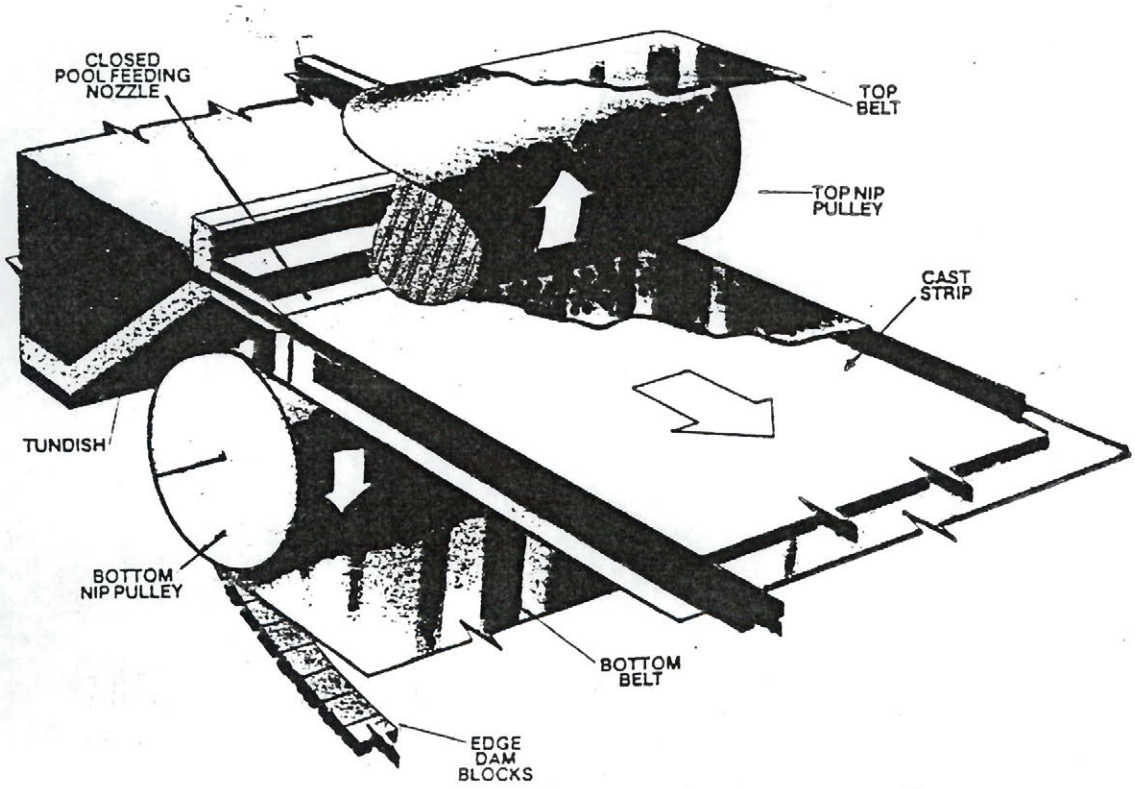

Figure (2.4) Closed-pool injection system[19].

The closed pool system is an important improvement in metal delivery where the molten metal surface can be protected or shrouded within the mould cavity from oxygen and other detrimental atmospheric gases[17]. The shrouding is by means of inert gas injected into the mould through a semi-sealing nosepiece, or directed at the mould cavity and passing through the

necessary slight gaps around the nosepiece. At the same time, such inert gas is further circulated so as to displace atmospheric gases from the casting belts as they approach the nosepiece before entering the mould region.

This technique required that the mould entry be completely covered, and visual access to the mould was obscured; thus, it was necessary to use a mechanical, electrical, or magnetic indicator for the pool level. Hazelett has developed the PLI (Pool Level Indicator) which can sense the meniscus by means of a series of thermistors on the opposite side of the casting mould which transmit the information to a readout panel. This technique eliminated the need to observe the mould entry to regulate metal flow in the tundish[17].

2.4.2 Mould Stabilization by Belt Preheating

In operation continuous-casting moulds distort and change shape in response to internally generated thermal stresses. The stresses arise from differential thermal expansion of the mould as local regions, particularly near the meniscus, attain higher temperatures than other regions during casting. Mould distortion is an important aspect in continuous casting because, in combination with mould wear, it adversely affects surface quality and breakout frequency[22].

Mould distortion is a function of the thermal field that obtains in the mould which in turn depends on a large number of variables. To study some of these variables, *Samarasekera and Brimacombe*[22] used a mathematical mould to predict the steady-state isotherms in a copper mould at the meniscus, centre of the mould, and mould bottom for standard billet and slab casting operations. In all cases they found that the temperature field was characterized by a hot zone close to the meniscus where heat flux was a maximum as shown in Figure (2.5).

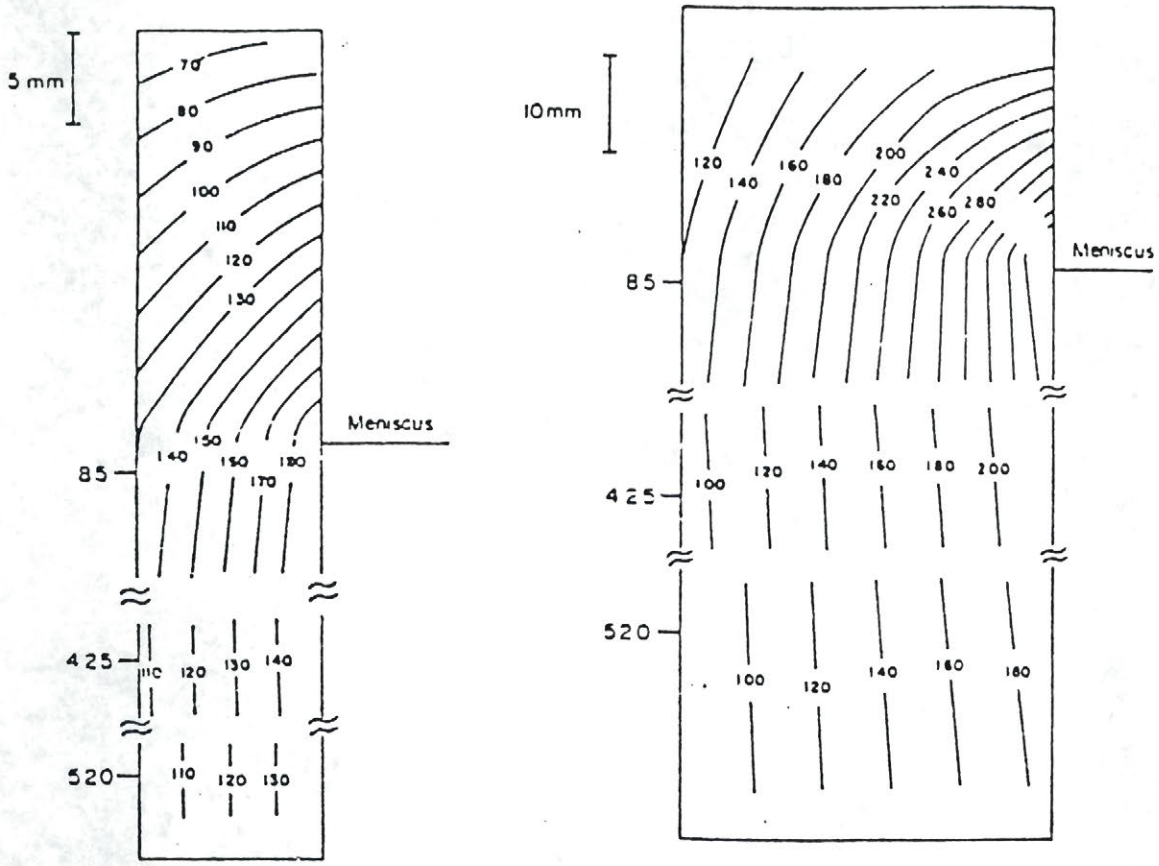

(a) (b)

Figure (2.5) Predicted steady-state isotherms in the wall a) a billet mould, b) a slab wall mould under standard conditions[22].

One of the attempts made to minimize belt distortion was the use of cooling water to cool the belts. It was found that accurate application of cooling water at the entry of the mould was a critical part of the twin-belt process[17]. Figure (2.6) shows the arrangement where the belt wraps around the entry pulley and begins its travel into the area where molten metal flows into the mould. Cooling water contacts the belt just prior to metal entry which is slightly downstream of the tangent point (i.e where the belt leaves the pulley).

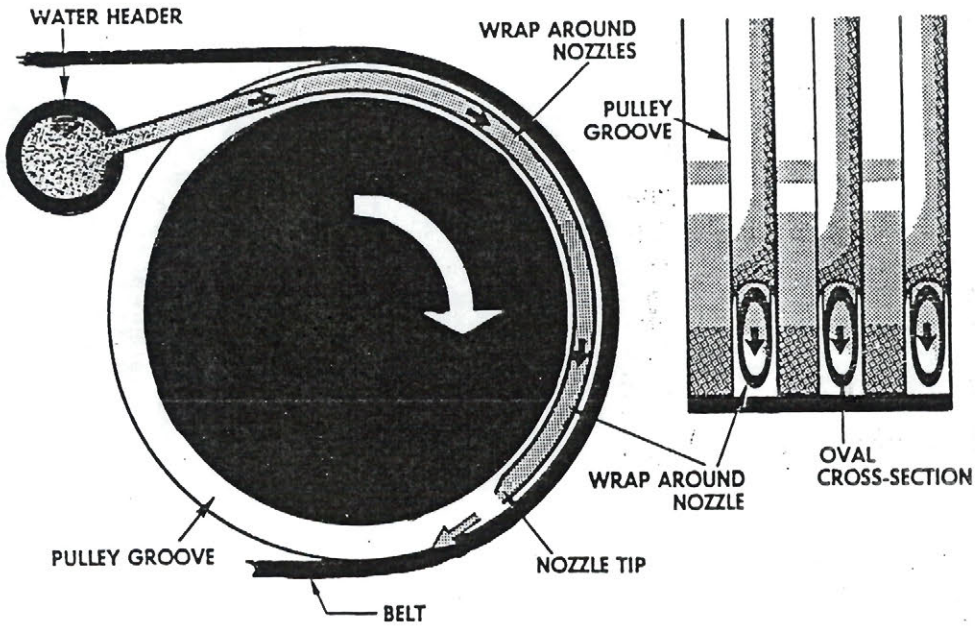

Figure (2.6) Water cooling system in the twin-belt caster[21].

The use of cooling water produced better results, but belt distortion was still a major problem. This occurs when molten metal enters the thin, water-cooled belt mould, the belts expand slightly due to a temperature increase occasioned by the heat transfer rate as the casting solidifies. The crux of the problem was seen to be the temperature difference through the belt as existing before the belt encounters the molten pool and after. The effect of these temperature differences, both in the belt and before and after metal entry, is to induce transverse buckling in the belt as shown in Figure(2.7)[21].

The longitudinal expansion is compensated by the tension generated by the outward pulley movement, but the transverse expansion is not compensated. Moreover, the belt edges restrain and limit any transverse belt movement.

Figure (2.7) shows the longitudinal and the transverse belt temperature profiles. The longitudinal profile, *(a)*, illustrates the temperatures in the belt as it moves into the hot casting region while the transverse belt profile, *(b)*, at a position several inches inside the mould.

The next step taken to minimize belt distortion was to preheat the belt prior to molten metal entry before applying cooling water. When belt preheating was applied (by applying steam at the water side) the belt pre-expanded, as shown in Figure (2.8), and less heat distortion took place when molten metal entered the mould[21].

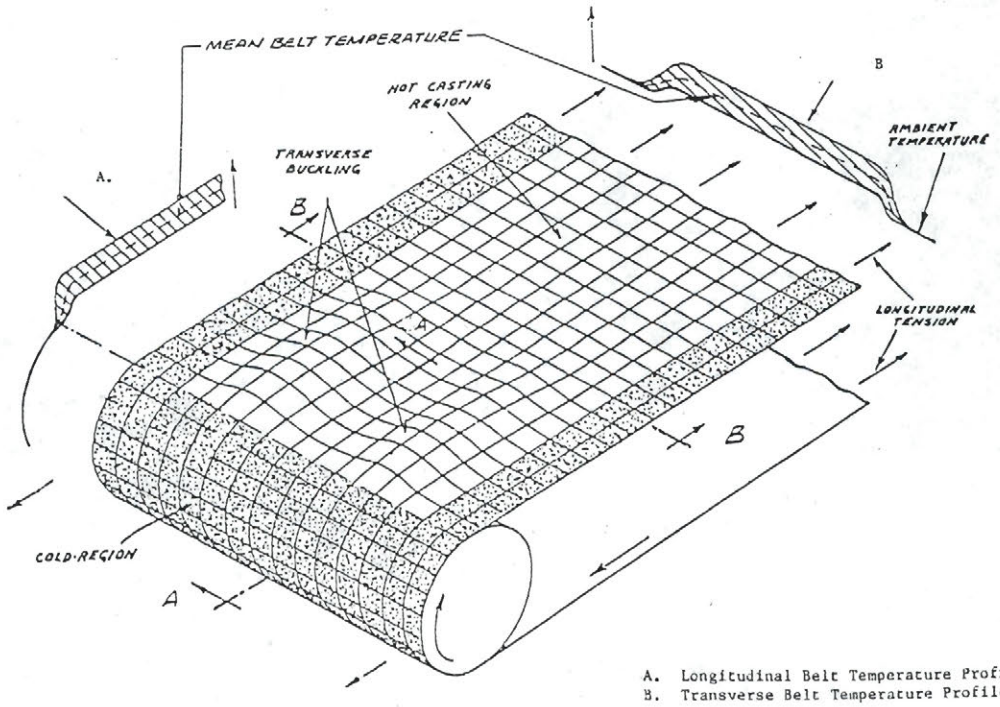

Figure (2.7) Belt schematic without preheating[21].

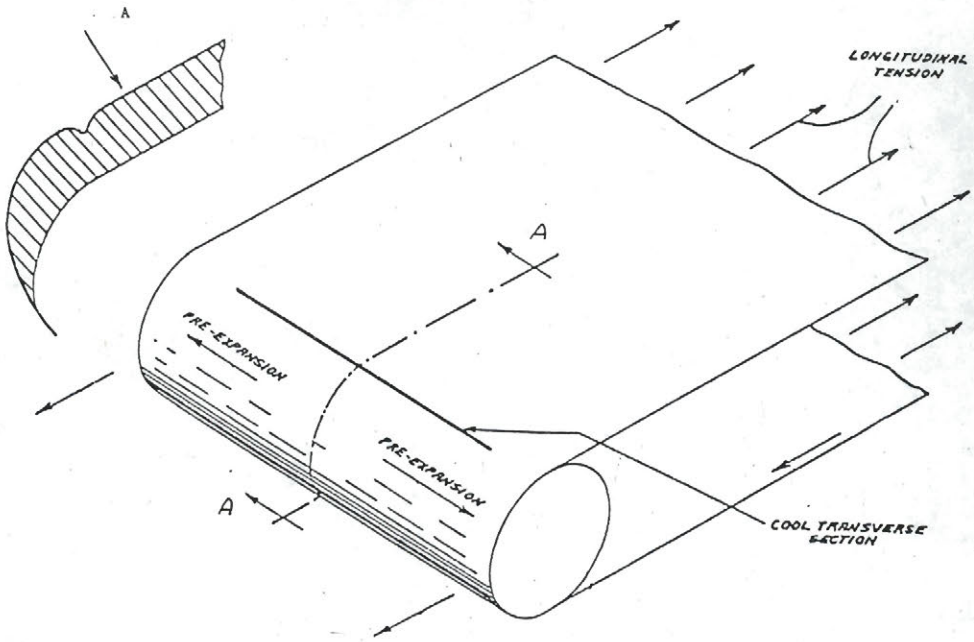

Figure (2.8) Belt preheating schematic[21].

(*A* represents a longitudinal temperature profile)

2.4.3 Belt Coating

Spray coating of the casting belt renders its surface rough. The effect of belt roughening on the casting parameters and the quality of the cast product can probably be understood by the consideration of the wetting phenomenon.

2.4.3.1 Basic Concepts in Wetting

The wetting phenomenon on a solid-liquid interface is frequently observed in daily life and is an important factor to be considered in metal casting.

Wetting processes involve the motion of a liquid interface along a solid surface which it contacts. The flow along the liquid interface near a solid-liquid-gas contact line is produced by the action of intermolecular forces on the liquid near the contact line. Whether flow is toward or away from the contact line depends both on the relative magnitude of liquid-liquid and liquid-solid intermolecular forces and on the size of the contact angle[23]. *Lopaz, Miller, and Ruckenstein*[24] state that the spreading rate of a liquid drop on a solid substrate is controlled by the balance between viscous resistance to flow and a single dominant driving factor, either the surface tension forces near the drop's periphery which tends to make the drop spherical, or gravity which tends to flatten it. *Nikolopoulos, Ondracek, and Sotiropoulou*[25] state that, along with the effect of the interfacial energies of the phases in contact, temperature is another factor affecting the spread rate of a liquid on a solid surface.

The main experimental methods used, to date, to characterize wetting of a solid surface by a liquid metal is the sessile drop method, where a drop of metal is allowed to rest on a plane substrate of the solid. In this method, wetting is characterized by a single scalar, namely the wetting angle, defined as the angle between the tangent to the drop surface at its line of contact with the substrate, and the substrate plane, measured through the metal as illustrated in Figure (2.9).

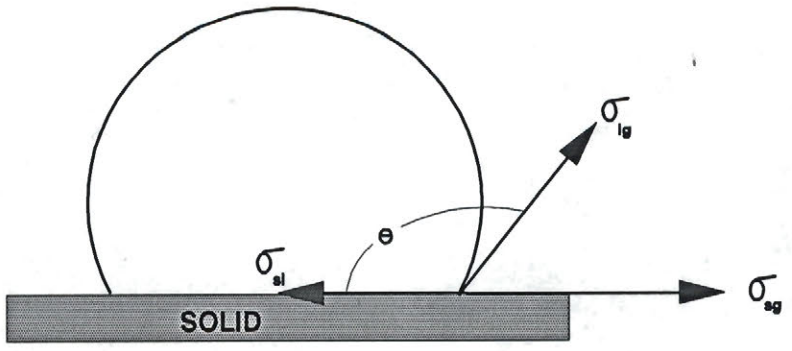

Figure (2.9) Contact angle in solid-liquid-gas system.

The wetting angle and the metal surface tension are linked with relevant surface energies by the Young-Dupré Equation[26];

$$\sigma_{sg} - \sigma_{sl} = \sigma_{lg} \cdot \cos\theta \qquad (1)$$

where; θ is the wetting angle, σ denotes the interfacial energy between two phases, which are indicated by subscripts s, g and, l for the substrate, the atmosphere and, the liquid metal, respectively.

Several methods are used to measure the surface tension of a liquid. For most determinations of σ, one or more of the following methods have been used:

a) Capillary Rise Method,
b) Maximum Drop Method,
c) Maximum Bubble Pressure Method,
d) Sessile Drop Method,
e) Pendant Drop Method,
f) Drop Weight Method,
g) Oscillating Drop Method.

Of these methods, the sessile drop method and the maximum bubble pressure method are most easily applied at elevated temperatures and have been most frequently used. The sessile drop method allows for more accurate determination of surface tensions over wide ranges of temperature compared with other methods used at high temperatures[27]. However, In order to use this method, every precaution must be taken to ensure the absence of any source of contamination. An adequate cylindrical symmetry of the sample, as well as good optical equipment are necessary before accurate data can be obtained.

Several equations have been presented to calculate surface tension from the dimensions of a sessile drop. Figure (2.10) shows the dimensions to be measured.

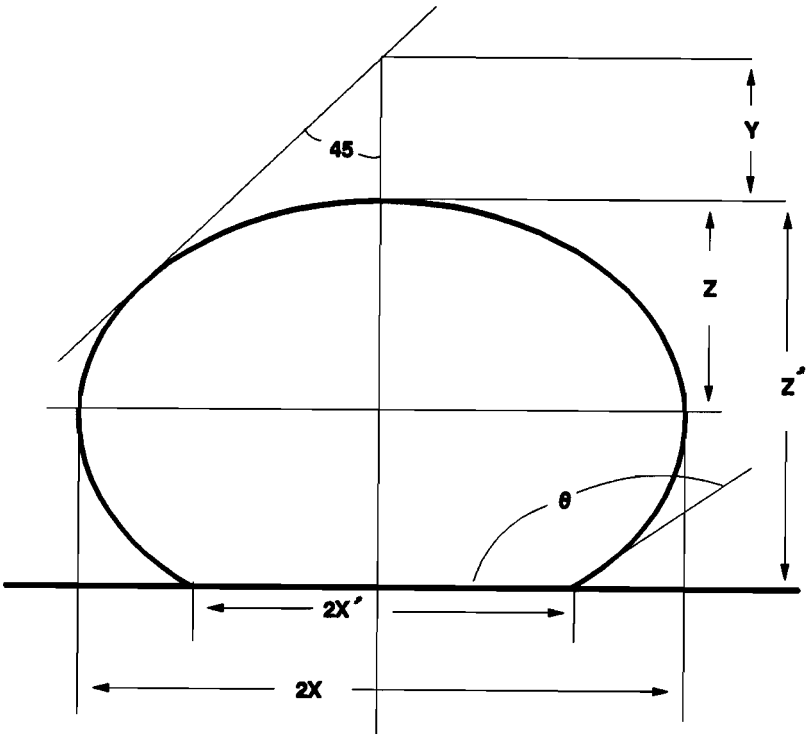

Figure (2.10) Measurements of sessile drop for surface tension calculations.

i) Bashforth and Adams equation The surface tension of the liquid specimen can be obtained using the Bashforth and Adams (1883) equation (see, e.g. Kingery and Humenik 1953):

$$\sigma_{lg} = g \cdot \rho \cdot b^2 / \beta \qquad (2)$$

where ρ is the liquid density. From measured values of X and Z, parameters **b** and β can be determined using the Bashforth and Adams (1883) tables. The difficulty in measuring Z entails an error of 2-3 per cent on σ.

Incidentally, the drop volume V can be calculated from the relation:

$$V = \pi \cdot b^2 \cdot (X')^2 / b \cdot (2/b - 2\sin\theta/X + \beta \cdot Z'/b^2) \quad (3)$$

Density can be obtained from the drop volume and its weight.

ii) Dorsey equation In this approach, the surface tension is calculated from the empirical relation, Dorsey's equation (Dorsey 1928):

$$\sigma_{lg} = g \cdot \rho \cdot X^2 \cdot (0.0520/f - 0.1227 + 0.0481 \cdot f) \quad (4)$$

where the Dorsey factor is given by

$$f = Y / X - 0.4142 \quad (5)$$

This method yields better accuracy than the previous one, but the difficulty in the experimental measurements of Y (Figure 2.10) remains an appreciable source of error.

iii) Corrected Worthington equation

$$\sigma_{lg} = 1/2 \cdot \rho \cdot g \cdot Z^2 \cdot (1.641\ X / 1.641\ X + Z) \quad (6)$$

The mathematical treatment of this equation (worthington 1885) appears to be satisfactory, but the difficulty in the determination of Z with high accuracy still remains.

In conjunction with the contact angle determination, a knowledge of the surface tension of the liquid leads to an expression for the work of adhesion, W_{ad}, of the two phases, which is given by[28] :

$$W_{ad} = \sigma_{lg} \cdot (1 + \cos\theta) \quad (7)$$

The work of adhesion represents the work done, or an increase in free energy, in separating the interface into separate surfaces of liquid and solid.

2.4.3.2 Effect of surface roughness on wettability

It has been known for several decades that the wetting of a solid surface by a liquid is affected by its roughness. Early studies with low energy solids and liquids showed that roughening decreased the spreading of the liquid[29, 30]. Wenzel[29] used a thermodynamic approach in which the additional surface area produced by roughening the substrate was regarded as effectively causing an increase in its surface energy and led to the prediction that;

$$\cos\theta_r = r \cdot \cos\theta \quad (8)$$

where; r is defined as the roughness factor, θ_r and θ are the contact angles on rough and smooth horizontal surfaces.

Dettré and Johnson[30] regard asperities as a series of energy barriers that must be overcome as the liquid front advances from one metastable configuration to another and spreads over the surface. The ability of a liquid to overcome such barriers and spread is regarded as depending on the relative sizes of its vibrational energy and the barriers[31].

More recently *Hitchcock, Carrol, and Nicholas*[32] investigated the influence of surface roughness on the wettability of high surface energy substrates, and particularly the wetting of ceramics by molten metals. In their investigation, they used the parameters R_a and λ_a to study the effect of surface roughness; where R_a is the average deviation in height of random points on

The Hazelett Corporation has lately been implementing the concept of surface roughness by using high-temperature materials such as ceramics to coat the casting belt. The use of a relatively heavy and sophisticated insulative belt coating of uniform thickness was acquired to reduce wettability between molten metals and the belt, reduce thermal belt distortion to an acceptable minimum, and decrease the high heat transfer necessary to fully cast the higher alloys.

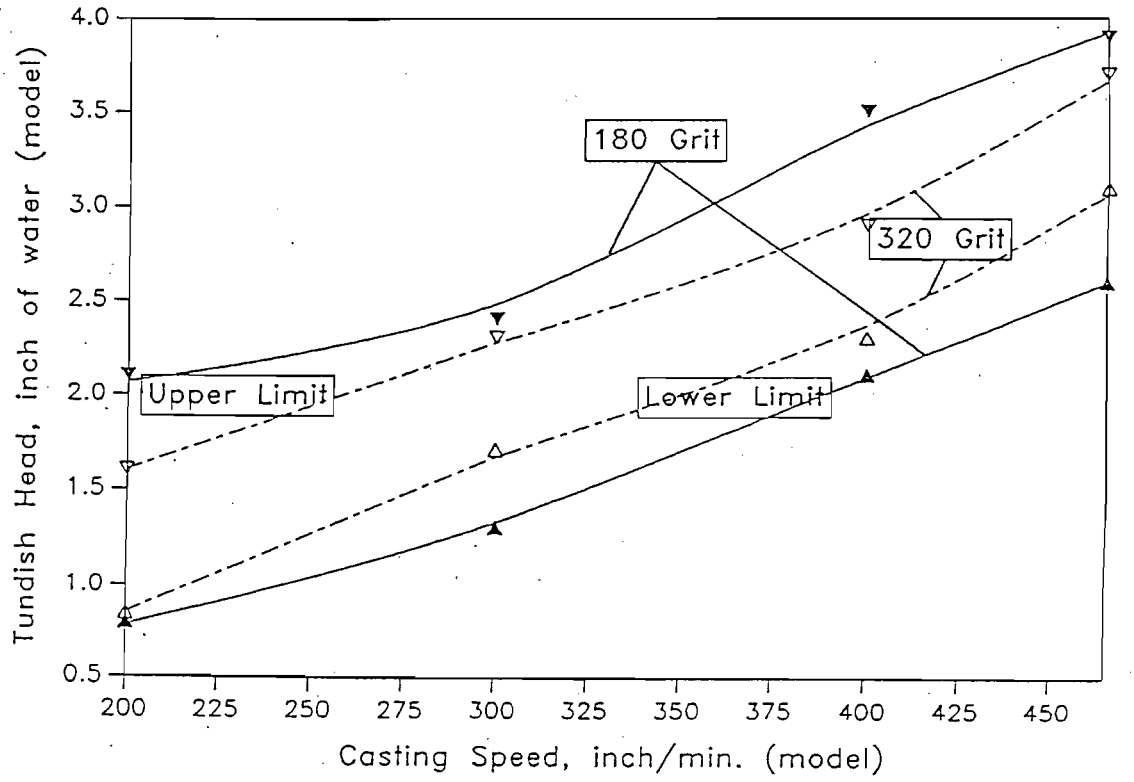

Figure (2.11) The effect of belt roughness on meniscus stability[33].

2.5 CERAMIC COATING TECHNOLOGY

Since the use of small amounts of high performance materials can significantly extend the operational range of inferior substrates, surface coatings are assuming an ever-increasing importance in many spheres of industrial activity. The following background on ceramic materials shows why ceramic materials are excellent candidates to serve as coatings for the casting belt.

2.5.1 Ceramic Materials

Ceramic materials have several unique properties. They are hard, chemically inert, dielectric, have high-temperature corrosion resistance and, make excellent thermal barriers. The ability to add all these qualities to a different base material as a thermally-sprayed coating overcomes many of the fabrication and brittleness problems of solid ceramics. On the other hand, with ceramic coatings metals become candidates for many applications for which otherwise would be unsuitable.

2.5.2 Ceramic-Coating Selection Criteria

The key concern for coatings that are expected to be applied in conditions of variant temperatures is the match of thermal expansion coefficients for the coating and the substrate. *G. Fisher*[34] states that for a satisfactory bonding of the coating, the thermal expansion coefficients must be within a factor of 1, (i.e., 1 x 10^{-6}/°C).

The crucial aspect of thermal expansion match is in preventing spalling of the coating as the composite goes through temperature cycling. For conditions where the coating has the lower

thermal expansion over the operating temperature ranges, small mismatches in thermal expansion coefficient result in the coating being in compression. Conversely, for substrates with lower thermal expansion, the coating experiences tension in thermal cycling, a condition generally resulting in cracking of the coating depending on the size of thermal expansion mismatch and the tensile strength of the coating[34].

Besides thermal expansion matching, coatings must not fuse with themselves, the mould, or the metal or bad casting surfaces will result. The coating must be such that no reaction with the mould or the metal occurs[35]. The ability of the coating material to withstand wetting by molten metal, and allow easy stripping of the casting from the mould, must be highly considered.

Other selection factors that must be considered when selecting a ceramic coating include: the service environment to be encountered by the coated metal, and the method of applying the coating[36].

2.5.3 Surface Preparation of the Substrate for Coating

Surface preparation is the most critical step in applying a ceramic coating. The coating strength is determined by how well it adheres to the substrate, and how well the coating particles adhere to each other[37]. Before a substrate is coated it must be 1) cleaned, 2) roughened. Surface cleaning can be achieved by vapour degreasing, oven baking or ultrasonic cleaning. Surface roughening is done by using the abrasive grit blasting method. The advantages of surface roughening are increased interlocking of coating laminations, increased bond area, and decreased surface contamination.

2.5.4 The Plasma Spraying Technique

Plasma spraying is considered to be the most universal coating technique. In this method, ceramic powders are introduced to an arc of partially ionized gas, (Ar, He, or N_2), that produces temperatures as high as 16649 °C [37]. The high-pressure plasma gas stream propels atomized molten ceramic particles onto a substrate. This method can spray ceramics of such high-melting point that are difficult to handle by the conventional flame spraying methods. The principle of plasma spraying is illustrated in Figure (2.12).

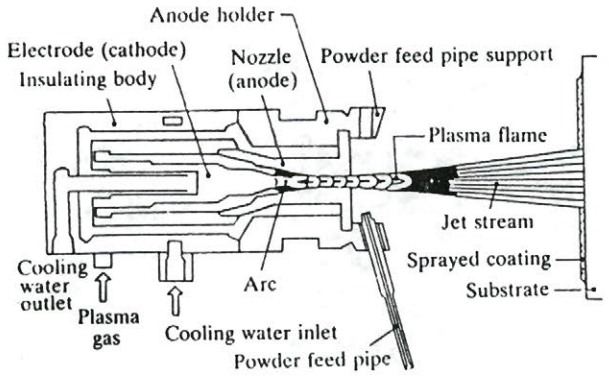

Figure (2.12) Plasma spray gun[38].

2.5.5 Basic Properties of Plasma Coatings

2.5.5.1 Structure

Plasma sprayed coatings exhibit a distinctive lamellar structure, which build up as the molten particles flatten against the substrate or material already deposited. Quenching rates, especially for the initial layers are estimated to be ~ 105- 106 k/s and so a fine-grained (or even amorphous structure, often containing metastable phases (i.e, Al_2O_3) develops within the splats[39].

2.5.5.2 Density and porosity

Porosity is a characteristic feature and structural index of sprayed coatings. The more viscous and faster the velocity at which the particles are sprayed, the denser is the coating structure. Ceramic coatings, being made from brittle and hard materials, usually exhibit high porosity. Porosity is undesirable if a wear resistance material is required. However, porous coatings of the same material are very suitable for thermal insulation. The pores occur on the grain boundaries, and their diameter varies from 20 to 100 μm.

The density of plasma coatings is lower than the theoretical density of the same material. It varies within 85 to 93 % [40].

2.5.3.3 Bonding and adherence of plasma coatings to the substrate

The process by which a coating sprayed on a substrate by plasma technology adheres is very complex and is still not fully elucidated and studied. *Matejka and Benko*[40] suggest that the effects of the following factors acting to create adherence:

a) mechanical anchorage of molten particles into the substrate;

b) contribution of physical interaction forces of the Van der Waals type;

c) Chemical interaction leading to microwelding of particles, i.e. formation of strong chemical bonds of a covalent or coordination-covalent type;

d) metallurgical processes, taking place in close vicinity to form microwelds.

However, the views of other researchers on this question differ considerably. Some authors believe that the processes taking place during spraying are too fast to allow the ***b***, ***c*** and ***d*** phenomena to occur, and, thus they ascribe the role to mechanical forces. In other words, the bond formation is played by mechanical catching of coating mass on the microuevennesses of the substrate.

2.5.3.4 Thickness and surface quality

Matejka and Benko[40] state that the coating thickness exerts an adverse effect upon the bond of coating with the substrate according to the following equation:

$$r_{subst} = - r_{coat} \cdot \delta_{coat} / \delta_{subst} \quad (9)$$

where; r is the radius of action of adhesive forces,

δ is the coating thickness.

Maximum stresses occur at the interface, and decrease in both directions with increasing distance from the boundary. Due to stress gradient, the forces acting normally tempt to tear off the coating from the substrate. The stress gradient in a thick coating is greater than in a thin one.

Figure (2.13) shows the distribution of stresses in the coating-substrate system in thin and thick coatings. The thickness of plasma-sprayed coatings of up to 0.5 mm are sufficient in many cases to protect engineering surfaces. Because of higher residual stress states in thick plasma-sprayed coatings, resulting from shrinkage between and within the splats as they cool, the security of the bond to the substrate reduces with the increasing thickness of the plasma-sprayed coating[41].

Due to the fact that the substrate surface has been roughened by grit blasting before spraying, the roughness of plasma-sprayed surfaces is in the same order of magnitude, although powder size is also a factor[42].

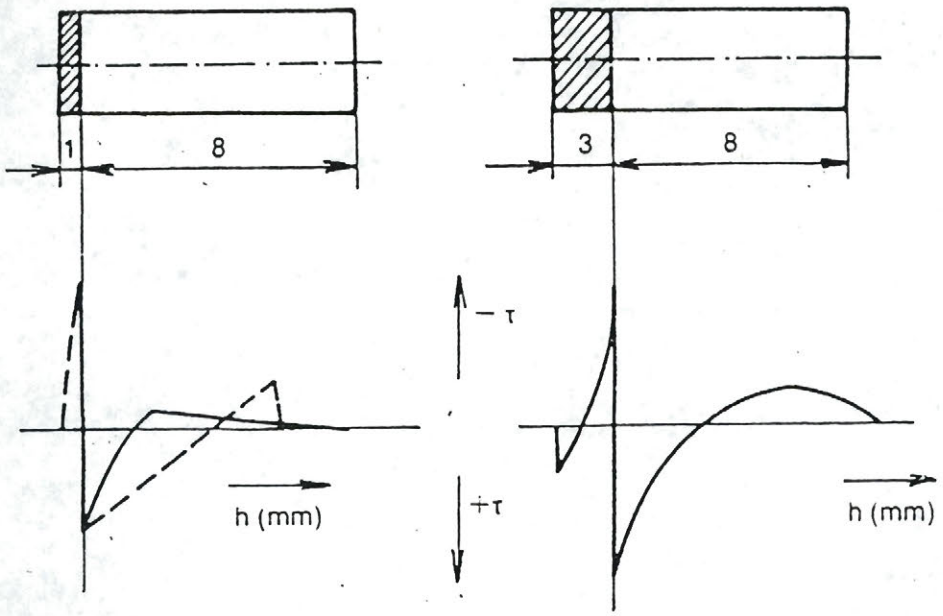

Figure (2.13) Distribution of stresses in the coating-substrate in thin and thick layers[40].

2.5.3.5 Heat Transfer

Heat transfer in a plasma sprayed coating can be realized in the following ways[40]:

a) by lattice or photon thermal conductivity in the particle, λ_f.

b) radiated photons in the coating pores, λ_c.

c) thermal conductivity of gas entrapped in the coating pores, λ_m.

therefore;

$$\lambda_{total} = \lambda_c + \lambda_f + \lambda_m \qquad (10)$$

Since heat transfer according to *c* proceeds slowly, a more porous coating would result in less heat transfer.

2.6 CERAMIC COATINGS STUDIED IN THIS WORK

2.6.1 Zirconia

Zirconia (ZrO_2) has a melting point close to 2482°C, with very good resistance to thermal shock. Zirconia is used as a thermal-barrier coating because of its low thermal conductivity (13.8 W/m.°K). The coating has a mean specific heat of about 7.3 X 10^3 J/kg.°K between 27°C and 1399°C. Its thermal-expansion rate is approximately 1.6 x 10^{-7} °C over the same range[37].

2.6.2 Stabilization of Zirconia

In the temperature range (ambient to 1400°C), pure zirconia undergoes a tetragonal to monoclinic phase transformation. This transformation occurs at approximately 1170°C, is accompanied by a 3-4% volume change. The increase in strain associated with this volume change makes pure ZrO_2 unsuitable for high temperature coating applications.

Oxides such as CaO, MgO and Y_2O_3 exhibit a high degree of solubility in ZrO_2, and can be used to partially stabilize the structure of ZrO_2 . Zirconia is alloyed with other oxides (stabilisers) so that the coating consists entirely of either the cubic or the tetragonal form at all temperatures to avoid degradation due to volume changes arising from transformations during heating and cooling[43].

The basic oxide is the major constituent of an oxide coating, usually being present in excess of 95 wt%. Other materials such as CaO, Y_2O_3, and MgO are added in small percentages for stabilization, increase of as-sprayed density, modification of surface characteristics, and improvement of resistance to thermal shock[36]. Thermal cycling results[44] showed that ZrO_2-MgO and, ZrO_2-Y_2O_3 coatings are more thermal shock resistance than ZrO_2-CaO coatings. The reason is that the MgO and Y_2O_3 coatings have less mean porosity ($\approx$ 15%). On the other hand

the CaO coatings contain excessive porosity, which induces premature spalling.

2.6.2.1 Yttria-Stabilized Zirconium Oxide

The 8%-yttria-stabilized zirconia has a melting point of 2649 °C and a thermal-expansion rate of 1.6 X 10^{-7} °C. This material retains its stability better than other stabilized zirconias, and thus is useful for long-term cycling applications[37].

2.6.2.2 Magnesia-Stabilized Zirconium Oxide

Magnesium Zirconate ($MgO.ZrO_2$) is a thermal barrier coating with high resistance to erosion by fine particles and molten metal. It has a melting point of nearly 2149 °C, and a thermal-expansion rate of 1.2 X 10^{-7} °C over the range of 21 - 1093 °C [37].

2.6.2 Alumina

Alumina (Al_2O_3) has a melting point close to 2050°C, with excellent abrasion resistance and good resistance to corrosion. Aluminum oxide is also a good thermal barrier; it can increase the temperature limit of a metal as high as 538°C beyond its unprotected use temperature[45].

2.6.3 Titania

Titania deposits (TiO_2) have high wear and temperature resistance. They have also a good corrosion resistance. The melting point of titania is about 2132°C [45].

From the above overview on ceramic coatings, one can apprciate the role these coatings play when applied to the continuous casting mould.

CHAPTER
THREE

MATERIALS, EQUIPMENT AND EXPERIMENTAL PROCEDURES

3.1 INTRODUCTION

In order to investigate a certain phenomenon taking place in a large industrial unit such as a metal caster, laboratory experiments can be set up to simulate those aspects of the industrial process that are of interest. These laboratory simulations can help in the understanding and solution of some of the difficulties encountered in industrial scale units.

The aim of this work was to study the wetting behaviour of two aluminum-manganese alloys and pure tin respectively, on Hazelett caster belts modified with plasma-coated ceramic substrates.

Experiments were also carried out on smooth copper and steel substrates simulating standard belts, in order to assess the effect of surface roughness on wettability.

3.2 MATERIALS

Since the tin and aluminum experiments were carried out using different equipment, this chapter deals with each set of experiments separately.

3.2.1 Tin Experiments

The purity of the tin used in these experiments was 99.99%. The plasma-coated substrates investigated are given in Table (3.1).

Table (3.1) Ceramic coatings used in experiments.

Matrix	Hazelett substrate index	Substrate type	Coating thickness
D	METCO-102	Titanium dioxide	6.0 mil P.S*
J	Baystate-pp42B	Zirconia**	3.0 mil P.S
Y	METCO-210NS-1	Magnesium zirconate	3.0 mil P.S
Z	METCO-101NS	Aluminum oxide	5.0 mil P.S

To investigate the wettability of tin on a smooth surface of a standard belt, the uncoated side of the ceramic-coated steel substrates was used as being representative of the uncoated steel belt. For the copper substrates, samples were taken from a copper belt used in the twin belt caster.

*** Plasma sprayed**
**** 8%-Yttria-stabilized zirconia**

3.2.1 Aluminum Experiments

In these experiments, Aluminum alloys 3003 and 3105 were used. The major composition of these alloys, along with their densities and melting-point range, are given in Table (3.2). The alloys were supplied by Alcan International. The substrates used to carry out the aluminum experiments were the same as those given in Table (4.1). The uncoated substrates used were also the same as those used for tin.

Table (3.2) Aluminum alloys composition.

Alloy	Composition (%)					Density	Temperature
	Cu	Mn	Mg	Fe	Al	(g/cm^3)	range (^oF)
Al 3003	0.12	1.2	--	--	rem.	2.73	1190-1215
Al 3105	--	0.6	0.5	0.5	rem.	2.71	1175-1210

3.3 EQUIPMENT AND PROCEDURES

3.3.1 Tin Experiments

The ceramic coated surfaces were used in the as-received condition, whereas each of the steel and the copper substrates was placed in a hydrofluoric acid solution (49% concentrated) for about 10 minutes, and then rinsed with acetone to remove the oxide layer.

A tin sample, in the order of 1 gram, was placed on the substrate to be investigated. The substrates used were in the form of square plates measuring (5mm X 5mm). A horizontal tube furnace, (Figure 3.1), was used to carry out the wetting experiments. The furnace consisted mainly of an $Al_2O_3.SiO_2$ tube incorporating two windows enabling the sessile drop to be illuminated and photographed. The ends of the furnace were water cooled to protect the furnace windows, and to allow the sample to remain cold inside the furnace until the set-point temperature was reached. The furnace was connected to an inert gas supply (pure Ar) and an oil diffusion pump allowing a vacuum of up to 10 X 10^{-3} torr.

The two set-point temperatures, chosen for this work, were 300 and 690 °C. The first-set point was chosen because it is close to the metal's melting point (232 °C), whereas the second set point was chosen for the sake of comparison to the aluminum experiments. The precision of the temperature measurements, carried out using a thermocouple, was found to be $\pm$5°C. For each system and set-point temperature, two to four experiments were carried out. Each experiment lasted about 20-30 minutes.

The procedures followed for these experiments were as follows:

1) The tin sample was cleaned by acetone, and then placed on the substrate.

2) The substrate, supported by a graphite stand, were inserted into the cold region of the furnace and levelled, and, the furnace windows were closed.

3) The furnace was then evacuated to about 30 X 10^{-3} torr.

4) After degassing, high purity argon was allowed in, at a rate of 260 ml/min., as the experimental atmosphere.

5) The furnace was turned on, and when the set point was reached, the substrate was pushed, via a glass rod, into the hot region of the furnace.

6) Upon melting, the metal assumed a sessile drop shape. Photographs of the sessile drop were taken immediately after melting and at various subsequent time intervals, to ensure that

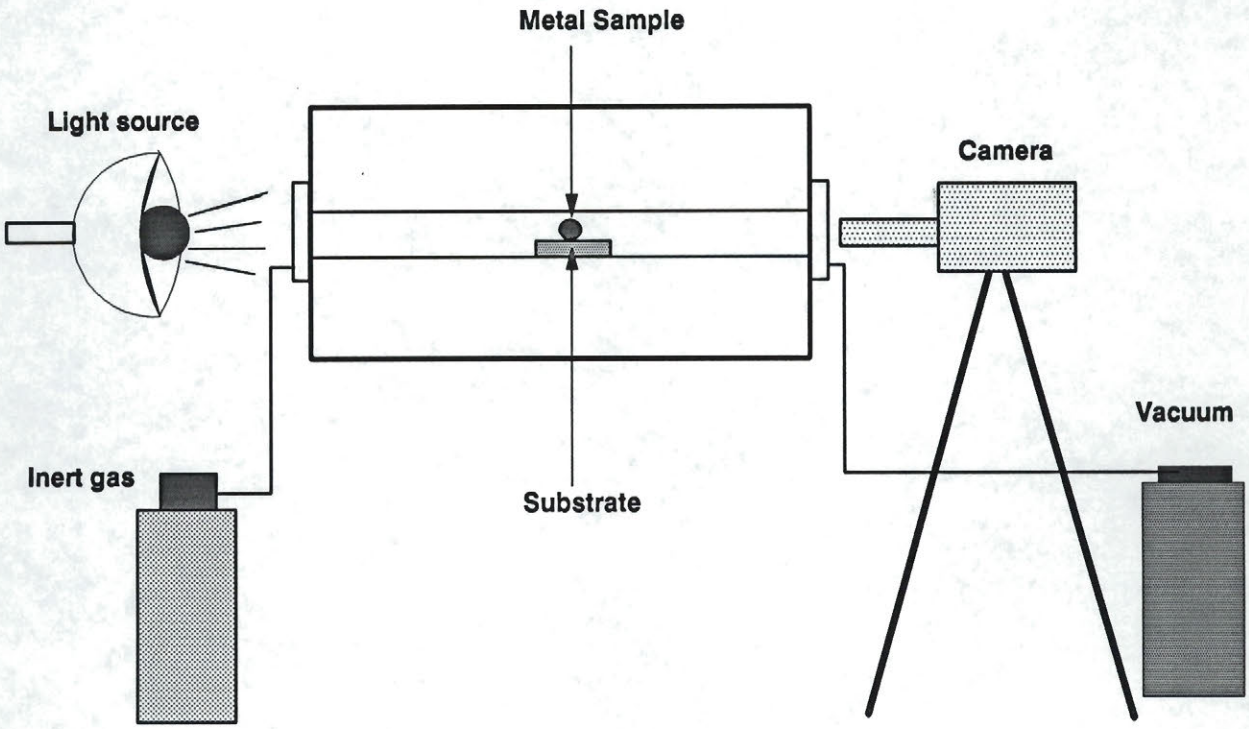

Figure (3.1) Horizontal Tube Furnace.

equilibrium had been attained. The melting conditions of the drop were kept constant during the experiments so that the results obtained could be compared.

5) Wetting angles were measured from photographic projections of the sessile drops.

3.3.2 Aluminum Experiments

Because of the relative ease of forming an oxide layer on the aluminum alloys, a tight vacuum system had to be used to obtain accurate data for contact angles of aluminum drops on substrates. A vertical tube furnace was used as shown in Figure (3.2). A schematic diagram of the full equipment is given in Figure (3.3).

The procedure for carrying out the experiments was as follows:

1) A graphite setup consisting of a reservoir, a cell, a platform, and a plunger was prepared. (See Figure (3.4)).

2) The substrate was placed in the graphite cell, and the aluminum samples placed inside the graphite reservoir. The cell was then tightened to the reservoir by means of a thread.

3) The graphite setup, with the aluminum sample and the substrate inside, was placed into the reaction tube of the resistance furnace. The tube was then closed, and the whole system evacuated to a vacuum level of 10^{-7} torr.

4) The system was then flushed with purified argon, this flushing procedure being repeated 3-4 times. Once a vacuum of 10^{-7} torr had been reached, power to the furnace was switched on and the reaction zone temperature was increased at a rate such that a vacuum of 10^{-7} torr was maintained at all times, during degassing.

5) Since the pouring temperature, used to cast aluminum alloys on the twin-belt caster, is 690°C, this temperature was chosen as the working temperature for these experiments.

6) The furnace was turned on, and when the set-point temperature was reached, a liquid sample of Al-3105 or Al-3003 alloys was squeezed by the graphite plunger. This plunger was pushed via a silica tube connected to a pushing screw. The oxide layer, coating the sample, was stripped off the bottom of the aluminum alloy in the graphite crucible as it passed through a 0.8-mm orifice, to fall on the substrate to form a droplet. Small pieces of pure aluminum (99.999%), situated below the substrate's platform, served as an oxygen getter.

7) Drop shapes were photographed with an x-ray film at different time intervals, keeping the temperature constant at 690°C ± 4.

8) The furnace switch was turned off, and the drop was left to solidify on the substrate, inside the furnace, under the same atmospheric conditions mentioned above.

9) A last photograph of the drop was taken after complete solidification, i.e, at room temperature.

10) A computer program, written by a student at The University of Toronto[46], was used to measure the contact angle. The program, being a combination of ***the Incremental Loading technique*** and ***the Newton-Raphson method***, is a numerical solution for the values of surface tension and contact angle. In this program, contact angles are determined from a given set of points which describe the shape of an axisymmetric drop . In other words, the drop is digitized by measuring the coordinates of several points on its contour and two points connecting the interface line. Samples of the results obtained, using this program, are given in Appendix A.

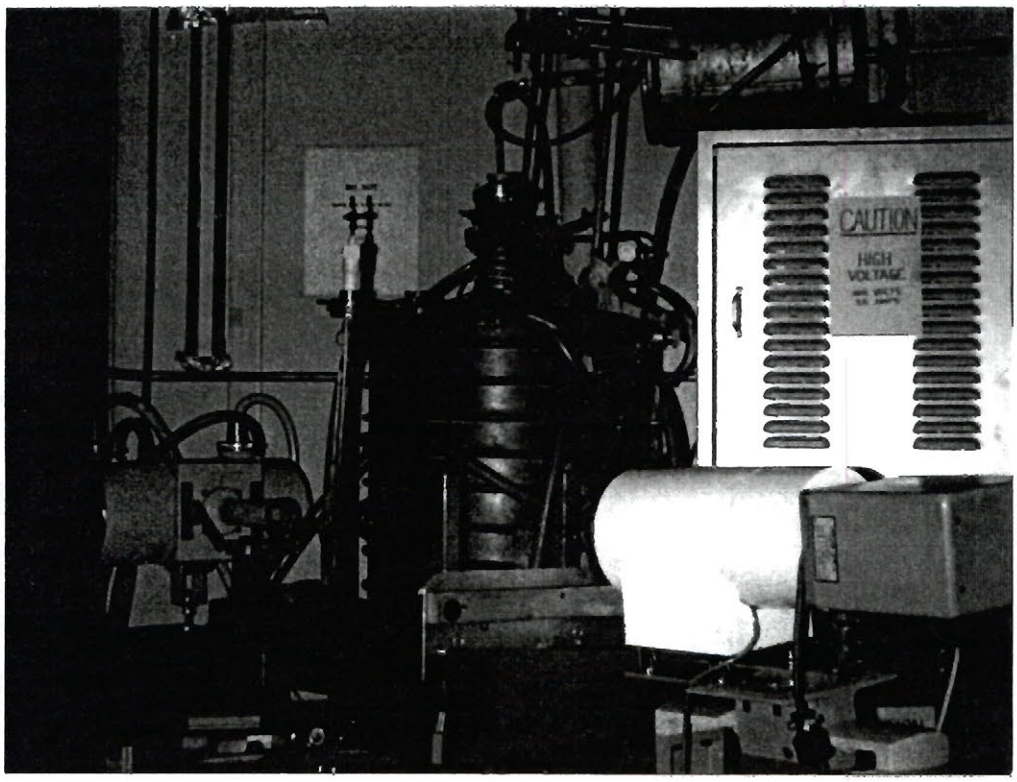

Figure (3.2) Vertical Tube Furnace.

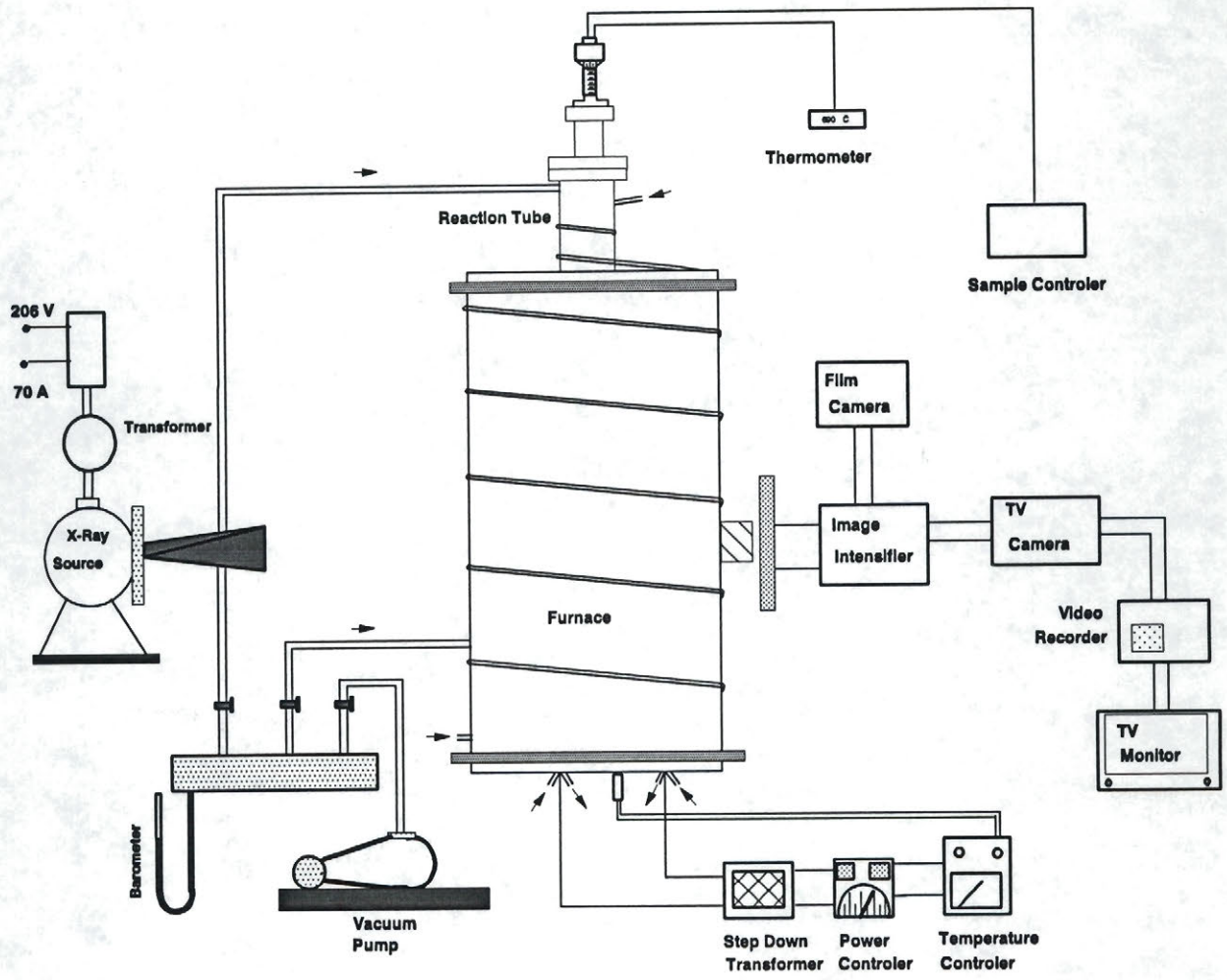

Figure (3.3) High Temperature X-Ray Radiographic Apparatus

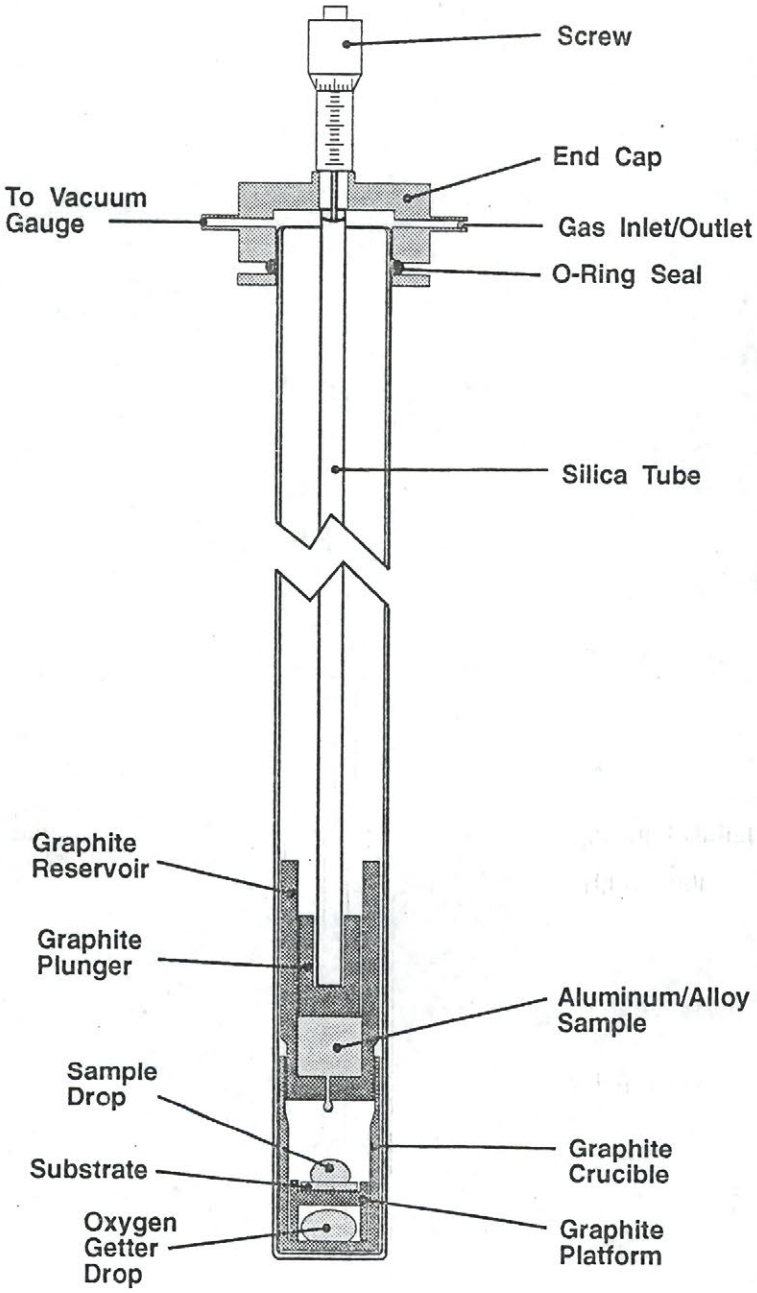

Figure (3.4) The graphite Setup.

CHAPTER
FOUR

DISCUSSION OF RESULTS

4.1 STRUCTURE OF PLASMA-SPRAYED COATINGS

A scanning electron microscope, (model JEOL 840A), was used to study the microstructures of the as-received coated substrates. The surfaces of the ceramic coatings were metallized (gold plated); therefore altering their surface free energy. Microstructures of all the coatings investigated in this work, reveal a fine-grained lamellar structure, which is a characteristic of all plasma-coated materials. It can be seen from Figure (4.1) that some particles exhibit spherical geometry, while others are less distinct and seem to be agglomerates or sponge-like. Under ideal spraying conditions molten particles strike the substrate surface where they flatten and freeze. The actual degree of flattening depends on many factors such as particle momentum, the extent of melting, viscosity of the liquid, and wetting of the surface[47]. As they hit the substrate, some particles do not have a chance to melt totally, and therefore remain in a spherical form. From Figure (4.1d), it can be seen that titania contains more spherical particles than any of the other coatings.

The structure of all coatings can be considered to be a weak joining structure with microcracks between laminar grains. The cracks are produced after spraying because of the shrinkage during the cooling process.

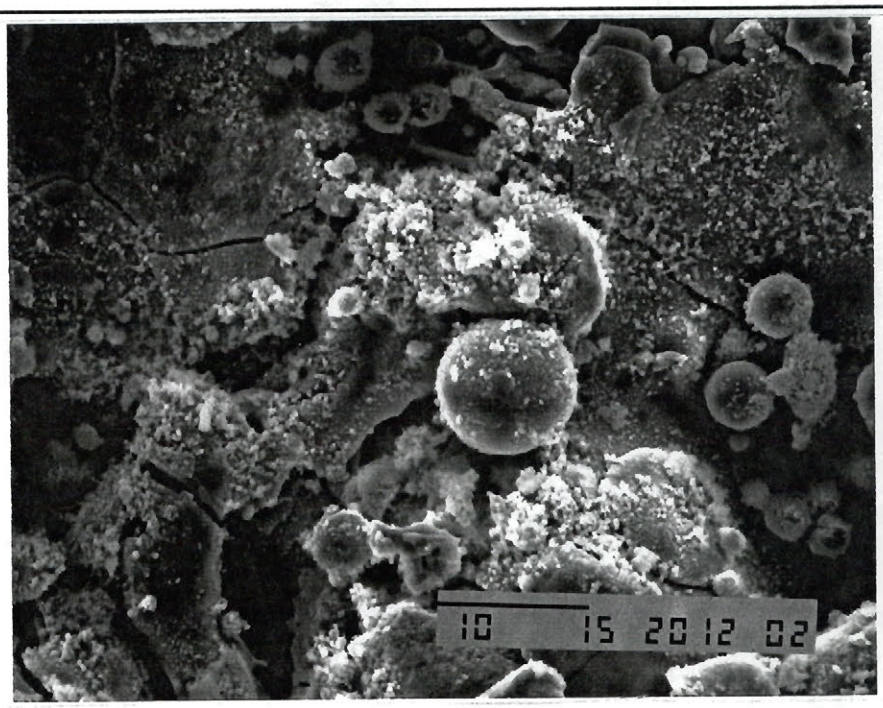

(a) Matrix Y (magnesium zirconate)

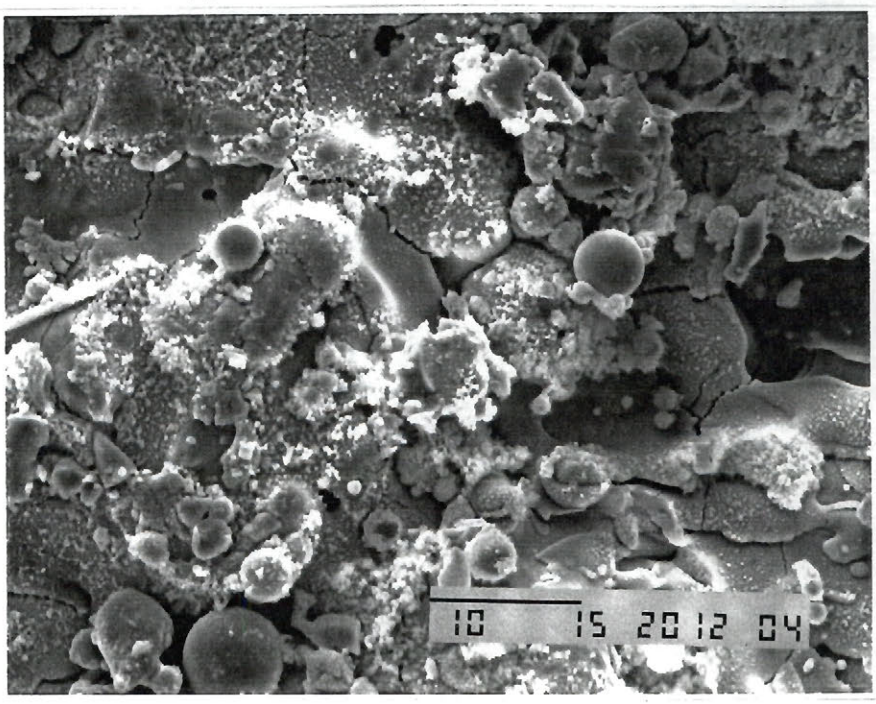

(b) Matrix J (zirconia).

Figure (4.1) SEM Micrographs of the Coated Substrates, (X 2000).

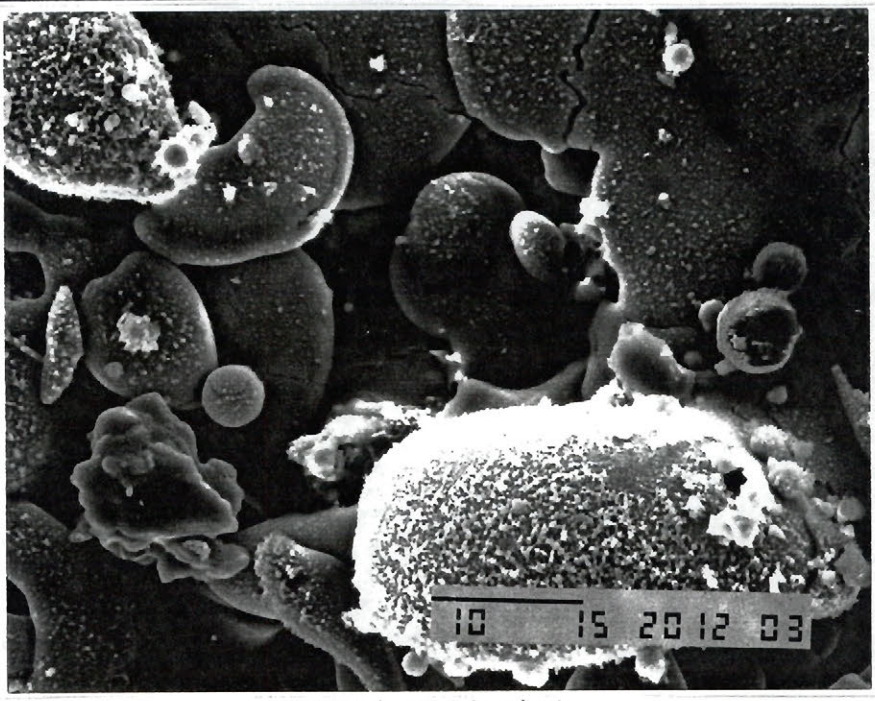

(c) Matrix Z (alumina).

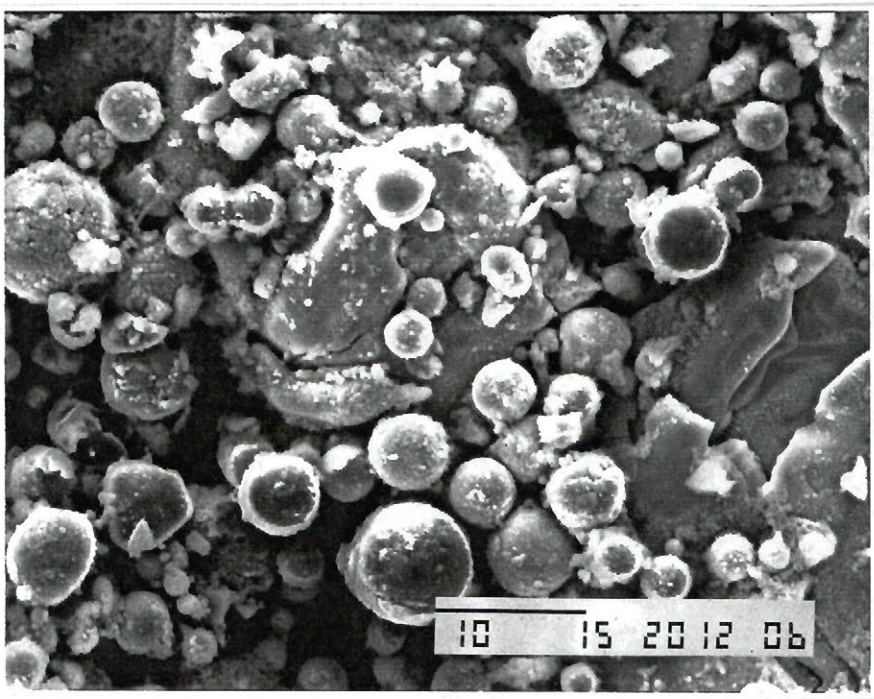

(d) Matrix D (titania).

Figure (4.1) cont'd, (mag.= X 2000).

A distinctive feature of all plasma sprayed coatings is their relatively high porosity compared to the corresponding compact materials. The coatings contain voids that probably resulted from outgassing, volatilisation, shrinkage, or topographical features. The open porosity of the coatings, used in this work, ranged from 30 to 40%. Porosity is an important feature of these coatings; since during casting the voids can be filled with gases that can slow heat transfer through the coating, hence delaying the solidification process, thereby preventing early solidification of the strand in the meniscus region.

4.2 OBSERVATION OF COATING-SUBSTRATE INTERFACE

A cross section of each ceramic-metal interface was mounted in a mould, polished, and then coated with carbon for about 20 minutes to prevent any charging that might occur during microstructural examination. The interfaces were then examined using a scanning electron microscope, (SEM model T300). As shown in Figure (4.2), all coatings appear to exhibit much higher porosity close to the mould surface, (along the interface), with a resulting higher thermal resistance, a phenomenon that may be attributed to the high rate of evaporation that takes place when the first layers of coating are sprayed.

The bonding efficiency between the coatings and the steel substrate appears to be low. Because of the rapid cooling, little interdiffusion can be detected between the coating and the substrate; bonding appears to be mainly physical in origin. It can be seen that all coatings contain cracks running parallel to the interface, with zirconia and titania showing the least, and the most, number of cracks, respectively.

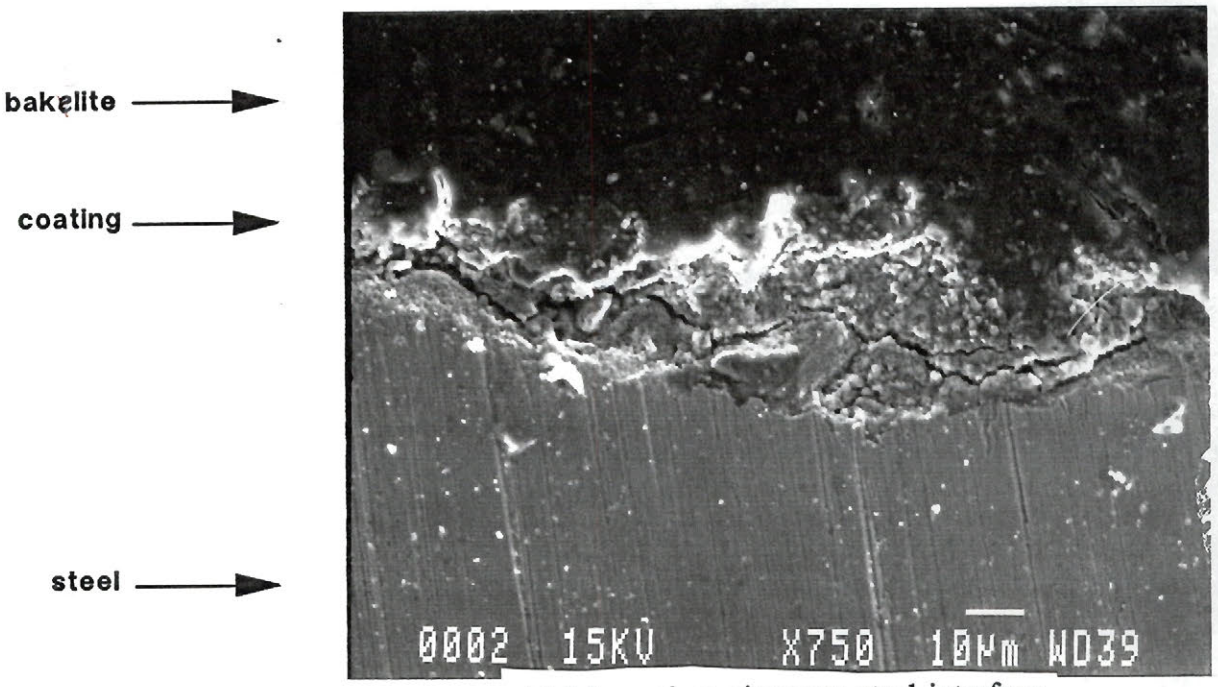

(a) Magnesium zirconate-steel interface.

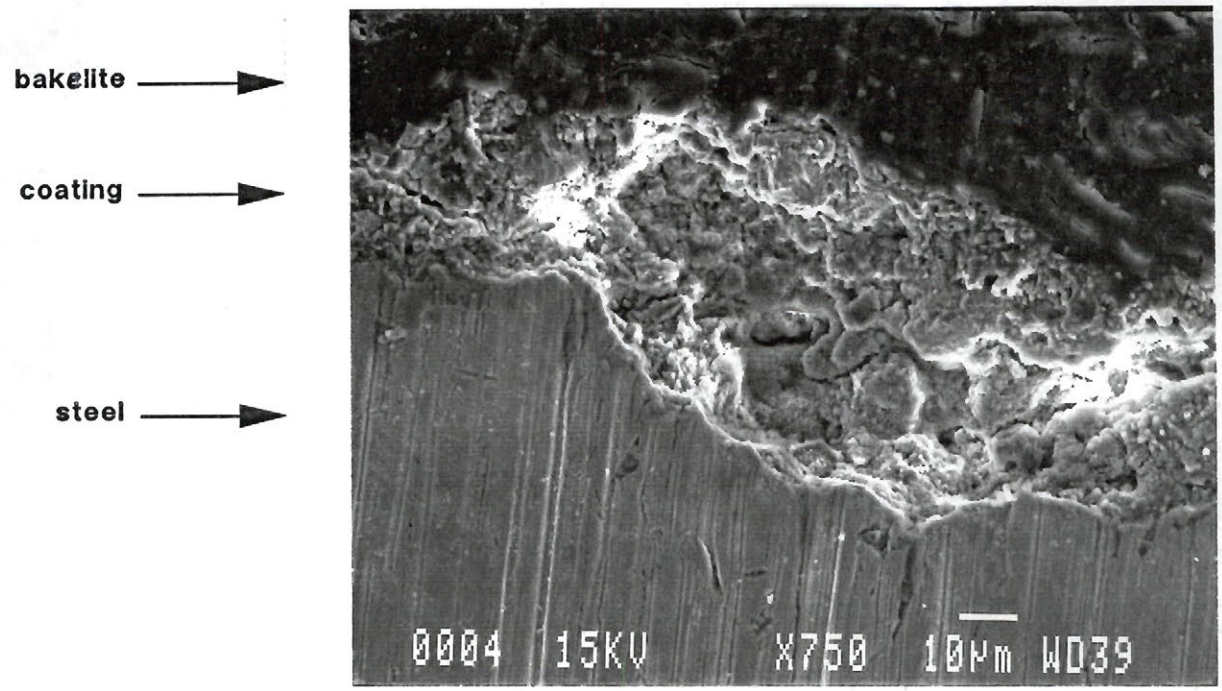

(b) Zirconia-steel interface.

Figure (4.2) SEM Micrographs of Ceramic Coating-Steel Interface.

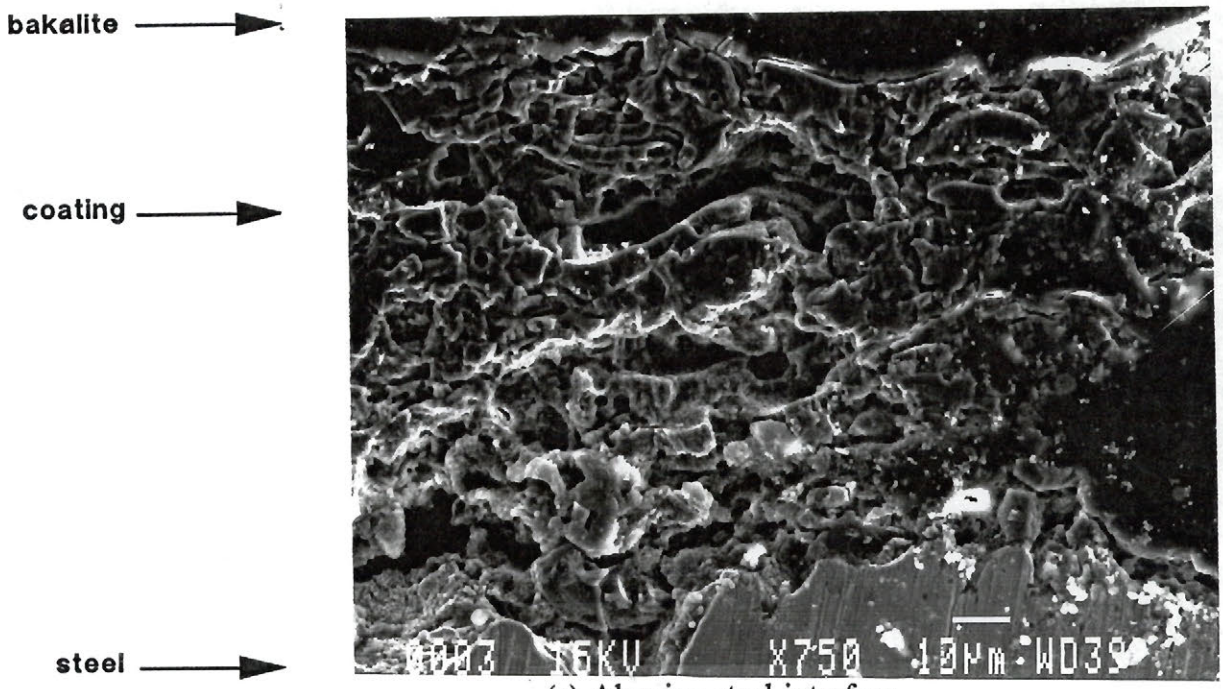

(c) Alumina-steel interface.

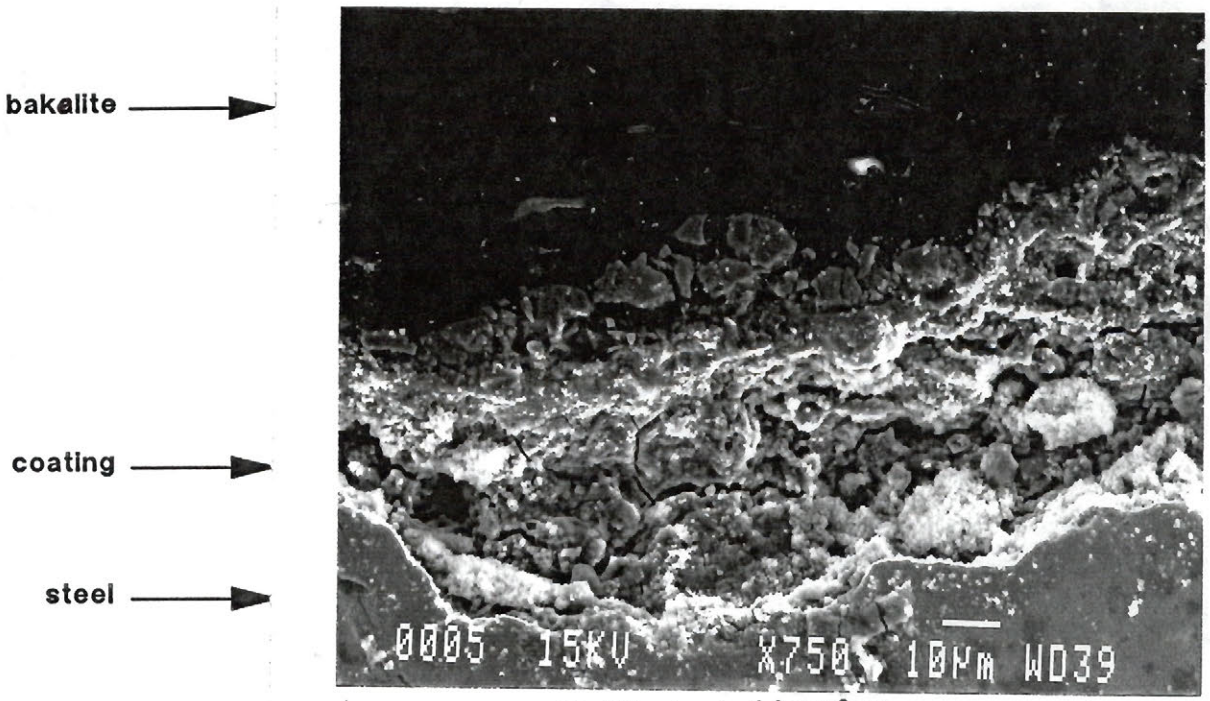

(d) Titania-steel interface.

Figure (4.2) Cont'd.

4.3 WETTING EXPERIMENTS

4.3.1 Tin Experiments

This wettability study was carried out on four coated substrates given in Table (3.1). Uncoated substrates of copper and steel were also investigated. Pure tin (99.99%), in the order of 1.0 gram was used for the wetting experiments. All experiments were conducted to determine the advancing contact angle assumed by a drop of liquid tin resting on each of substrates mentioned above.

4.3.1.1 Experimental temperature (300°C)

The wetting curves,for coated and uncoated substrates, are given in Figure (4.3). The corresponding numerical values are given in Table A1 of Appendix A. Experiments conducted on smooth (uncoated substrates) showed that the wettability of tin on copper was greater than that on steel. Two minutes after the insertion of the sample into the hot zone of the furnace, the contact angle of a tin drop on a steel substrate was 150°. The angle decreased slightly with time, reaching an equilibrium value of 146° after fifteen minutes. In the mean time, the contact angle, of a tin drop resting on a copper substrate, decreased from 112° to 98° in a time span of fifteen minutes.

Sessile drops of liquid tin on coated substrates assumed symmetrical profiles with contact angles finally being time-independent in all systems examined, suggesting that equilibrium had been achieved. Measurements of contact angles showed a slight or no decrease in contact angle with time. Since the error of measuring the contact angle was estimated to be $\pm 3°$, no apparent difference in wettability among the various coated substrates could be deduced.

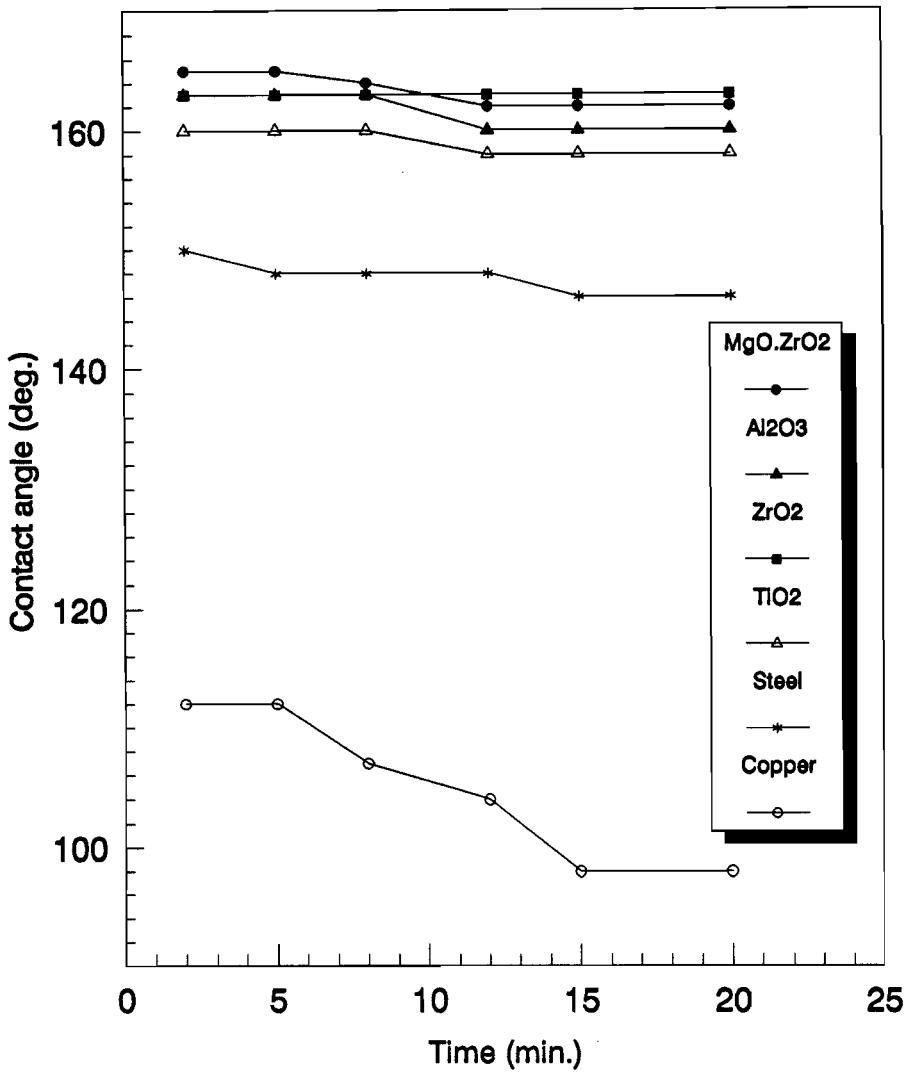

Figure (4.3) Contact angle vs. Time for Tin, (T=300°C).

4.3.1.2 Experimental temperature (690°C)

Contact angle measurements as a function of time, for both coated and uncoated substrates, are given in Figure (4.4). For exact numerical values see Table A2 of Appendix A. Compared to those conducted at 300°C, experiments conducted at 690°C showed a more pronounced difference in wettability between the copper and the steel substrates.

However, contact angles of tin drops on both substrates were relatively smaller than those obtained at 300°C. They ranged from 135 to 112 degrees for steel, and from 90 to 32 degrees for copper, in a time span of about fifteen minutes. After approximately fifteen minutes from the start of heating, contact angles on both substrates, became time independent; showing no measurable change with time.

For the coated substrates, contact angle measurements showed a more pronounced difference, among some of the substrates, than that exhibited at 300°C. As can be seen from Figure (4.4), titania (TiO_2) appears to be more wettable by tin than alumina (Al_2O_3), or magnesium zirconate ($MgO.ZrO_2$). Again due to the fact that the error in measuring contact angles was $\pm 3°$, no apparent distinction can be made regarding the difference in wettability between magnesium zirconate and alumina. Three out of four experiments, conducted on zirconia substrate, showed that zirconia was less wettable than titania, but more wettable than either alumina or magnesium zirconate. Figure (4.5) shows some of the sessile drops formed on the various substrates at 690°C.

At the two temperatures investigated, most of the contact angle measurements were reproducible within $\pm 3°$. The standard deviation of contact angle measurements ranged from 1.4 to 2.6 degrees.

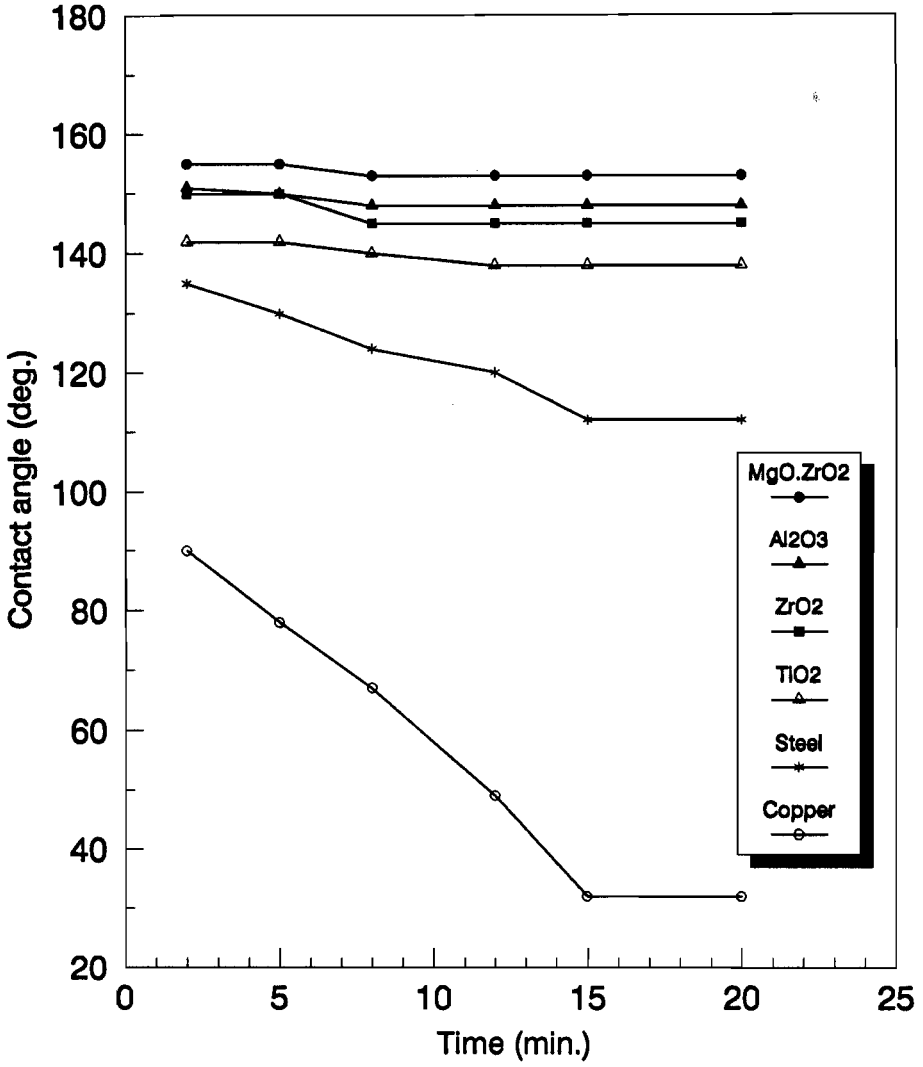

Figure (4.4) Contact Angle versus Time for Tin (T=690°C).

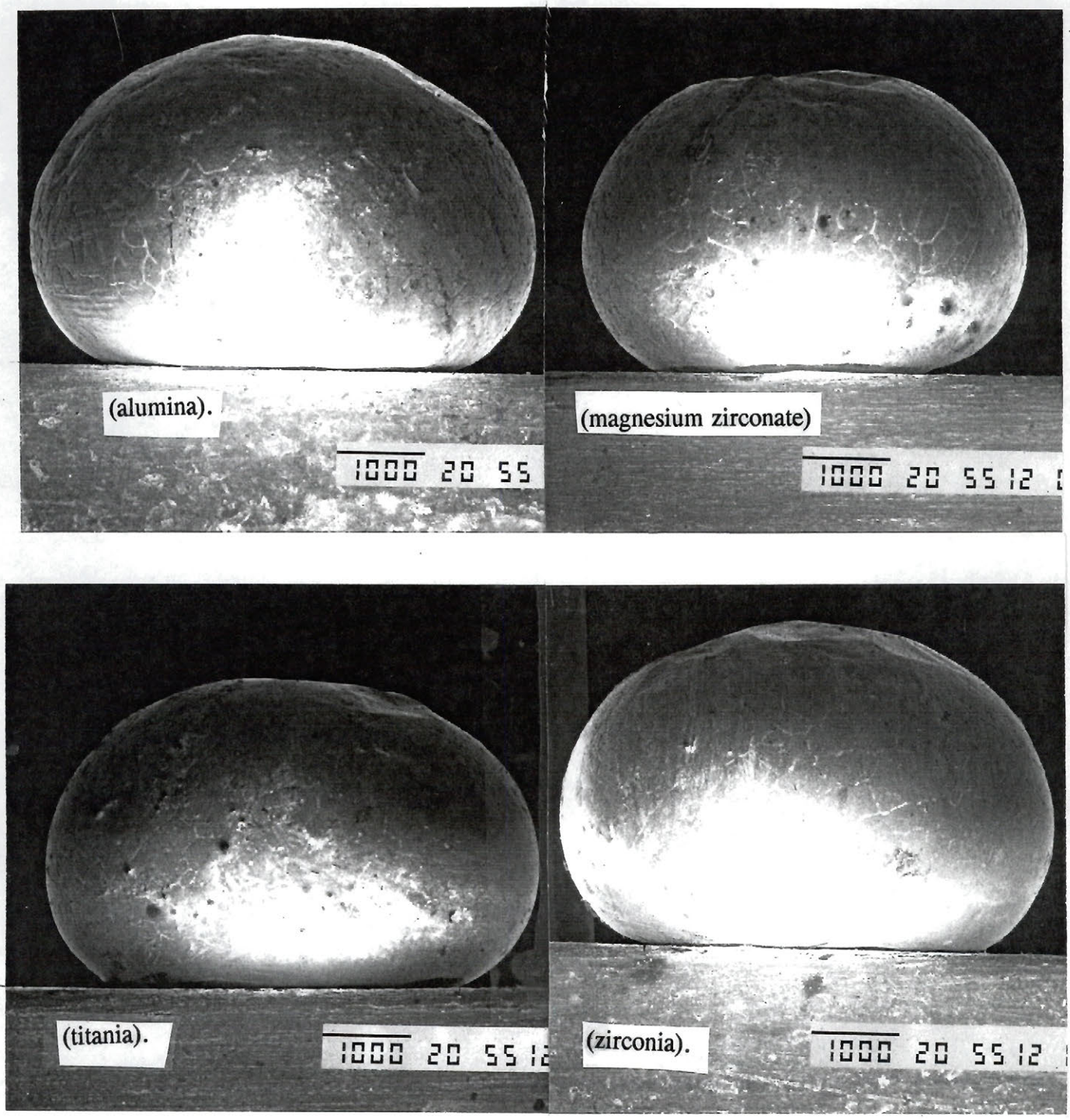

Figure (4.5) Solidified sessile drops of tin, formed at 690°C, on coated substrates, (X 15).

4.3.1.3 Analysis of Drop-Substrate Interface

After the wetting experiments, removing the solid drop from the substrate surface was attempted. Tin drops solidified on the coated substrates showed no adherence; the drops rolled off the substrate as they were being removed from the furnace. Visual examination of the interface side of the drops showed no apparent reactions between the drops and the coated substrates. On the contrary, tin drops, solidified on the copper and steel substrates, were attached to the substrates even after removal from the furnace. At both temperatures (300 and 690°C), the Sn-Cu system showed a strong adherence, suggesting that an intermetallic compound might have been formed. From Figure B1, (Appendix B), it can be seen that at the temperatures investigated, reaction products such as Cu_6Sn_5 and/or Cu_3Sn can form at the interface.

Figure (4.6) shows a microstructure of the interface region of a tin drop formed on a copper substrate at 300°C. A back-scattered electron microscope, used to determine the compositional variation at the interface, showed that the interface consisted of two regions. A rich-copper region (dark area) near the copper substrate, and a rich-tin region (light area) away from the copper substrate. As shown in Figure C1 of Appendix C, the dark area consisted of about 73 at% Cu and 27 at% Sn, whereas; the light area consisted of about 44 at% Cu and 55 at% Sn. Applying the concept of the lever rule, it was found that the dark region consisted of about 82% Cu_6Sn_5, whereas; the light area consisted of about 90% of Cu_3Sn.

The Sn-Fe system also exhibited a strong adherence between the drop and the substrate. In comparison to the adherence in the Sn-Cu interface, less force was required to separate the tin drop from the steel substrate. From Figure B2, (Appendix B), it can be seen that, at the temperatures investigated, the products FeSn and $FeSn_2$ may form at the interface. Although a spot analysis, at the interface, showed that it consisted of both tin and iron, suggesting the occurrence of some reactions at the interface, the individual reaction products could not be identified due to the very small thickness of the interface layer.

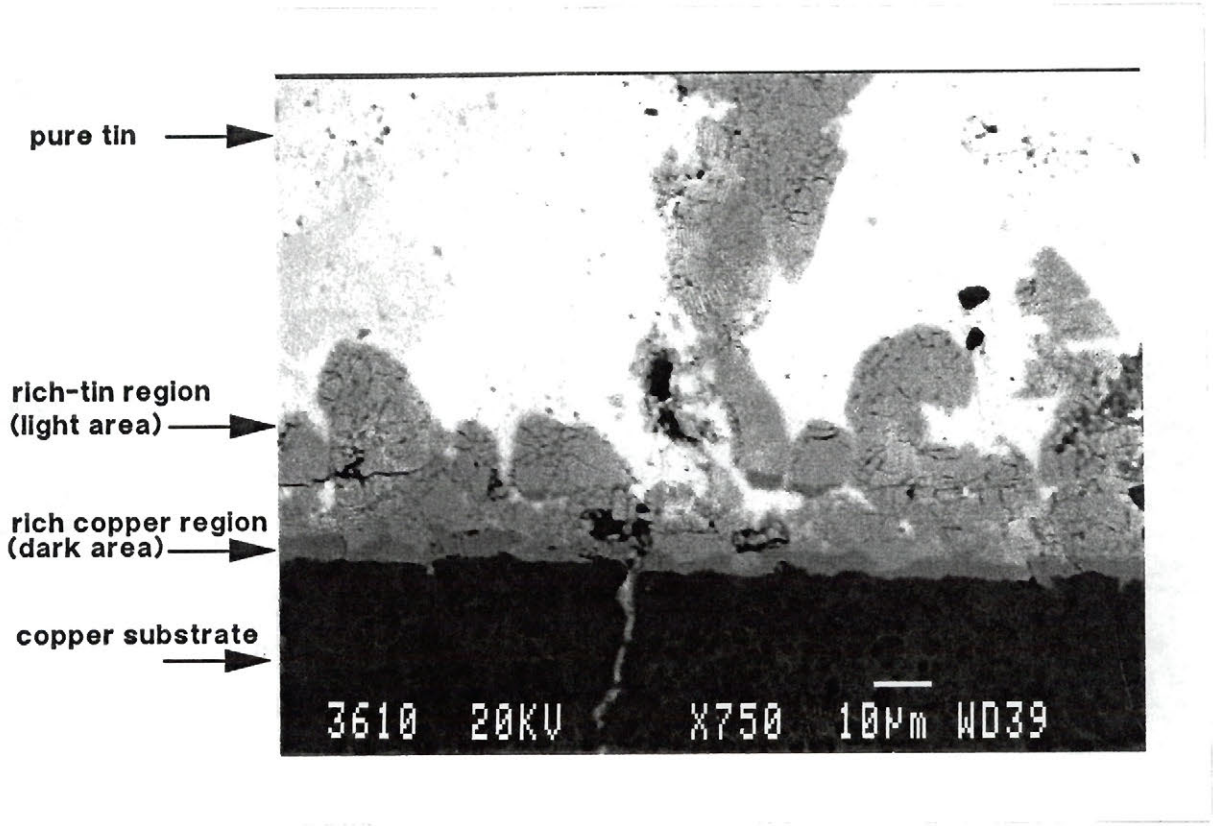

Figure (4.6) SEM Image of Interface in the Sn-Cu System.

4.3.2 Aluminum Experiments

The wettability of aluminum alloys 3105 and 3003 on the four coated substrates given in Table (3.1) and a steel substrate, was investigated. Contrary to the tin experiments where the tin drop was placed on the substrate before the start of the experiment, the aluminum drop was brought into the liquid state first, and then dropped on the solid substrate by means of the system illustrated in Figure (3.4).

4.3.2.1 Aluminum alloy 3003

Contact angle measurements of aluminum alloy 3003 on the steel substrate are given in Figure (4.7). For the corresponding numerical values see Table A3, Appendix A. A total of two experiments were conducted on the steel substrate. In each of the two experiment, the contact angle showed a gradual decrease with time up to about 10 minutes, and then reached a value of 115° where it remained constant for the rest of the experiment.

As illustrated in Figure (4.7), contact angle measurements of experiments, conducted on the four coating substrates, showed that the wettability of aluminum alloy 3003 on these coating decreased in the following order: titania, zirconia, alumina, magnesium zirconate. While the equilibrium contact angle for titania was 144°, those of zirconia, alumina, and magnesium zirconate were 156, 162, and 168°, respectively. Photographs of sessile drops of aluminum 3003, in equilibrium with the coated substrates, are given in Figure (4.8).

Comparison in wettability between the titania coating, and the uncoated steel substrate (equilibrium contact angle of 115°), clearly indicate that the latter exhibits more wettability than the former; a result that agrees with that obtained from the tin experiments.

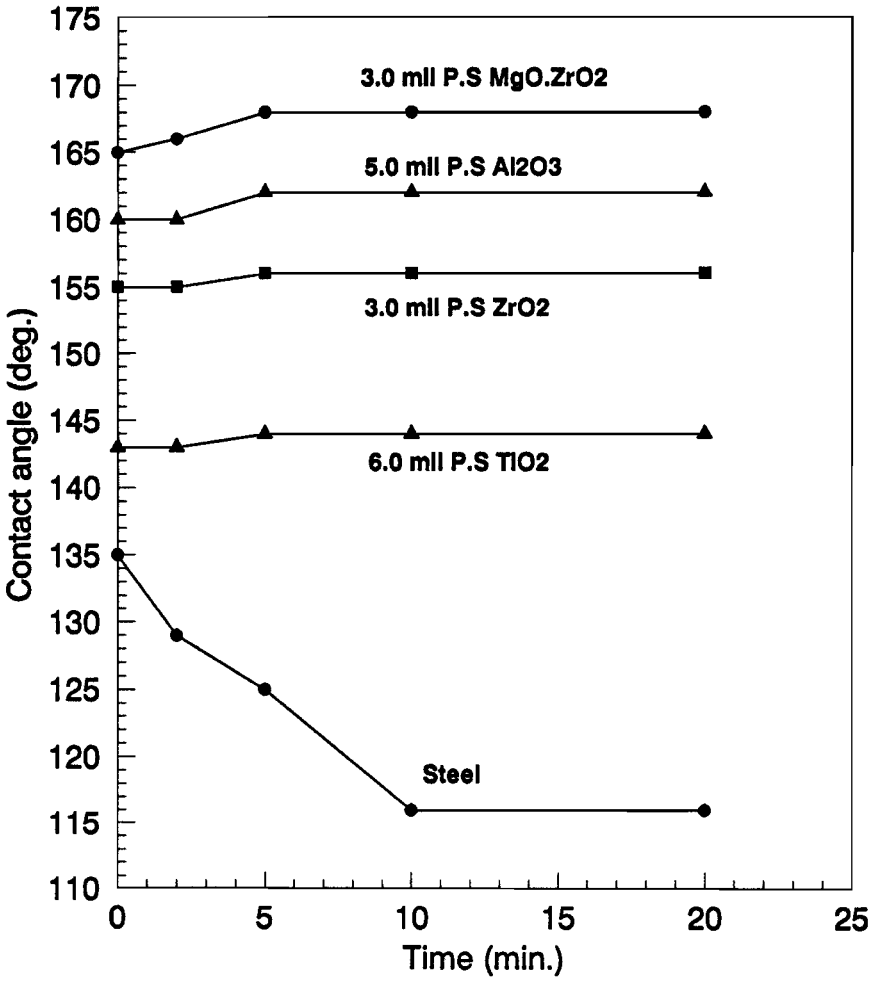

Figure (4.7) Contact angle versus time for aluminm 3003 on steel and ceramic-coated steel substrates, (T=690°C).

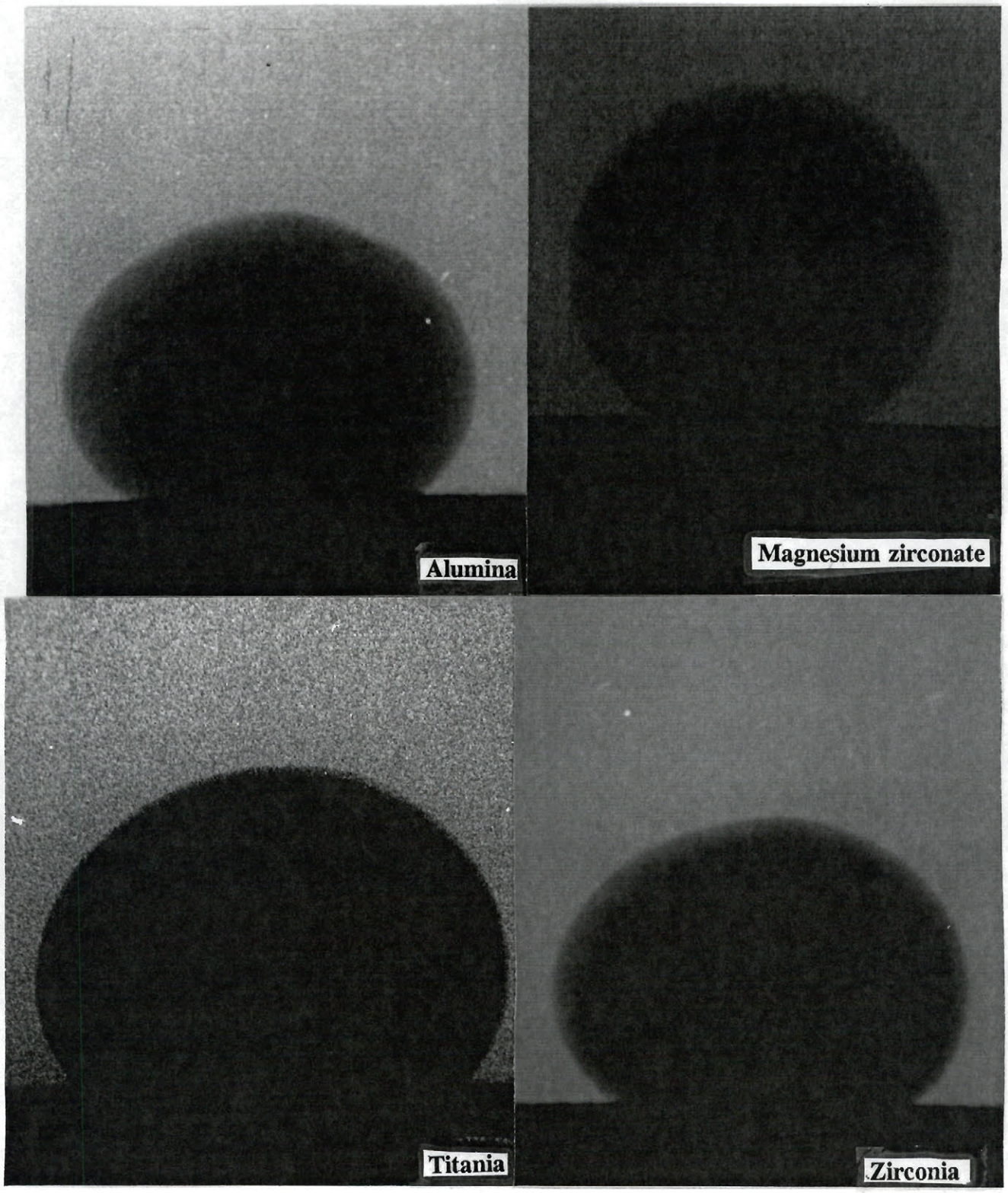

Figure (4.8) Photographs of Sessile drops of Aluminum 3003 on Coated Substrates.

4.3.2.2 Aluminum alloy 3105

Contact angle measurements of aluminum alloy 3105, on steel and coated substrates, are given in Figure (4.9) and Table A4 of Appendix A. A total of three experiments were carried out to study the wettability of aluminum alloy 3105 on a steel substrate. For all experiments, the equilibrium contact angle was reached after about 10 minutes (from the time the drop hit the substrate); with an average value of 119°.

Examination of contact angle measurements showed that, although all the substrates were not wettable by aluminium 3105 ($\theta > 90°$), magnesium zirconate, with an equilibrium contact angle of 160°, appeared to exhibit less wettability than any of the other coated substrates. Equilibrium contact angles, of alumina and zirconia, were 152° and 150°, respectively.

Since the reproducibility of the contact angle measurements, on all substrates, was $\pm 2°$, no distinction in wettability could be made between alumina and zirconia. Among the four coated substrates, investigated in this work, titania showed the highest wettability (equilibrium contact angle = 140°).

The wettability of aluminum 3105, on all coated substrates, appeared to be higher than that of 3003 on the same substrates. This *may* be attributed to the difference in the chemical composition between the two alloys.

For each alloy-substrate system, a photograph was taken of the drop after complete solidification. Contact angle measurements of the solidified drops were the same as the equilibrium values of the corresponding liquid drops; indicating that there was no effect of solidification on the value of the equilibrium contact angle. Photographs of sessile drops of aluminum 3105, in equilibrium with the various coated substrates, are given in Figure (4.10).

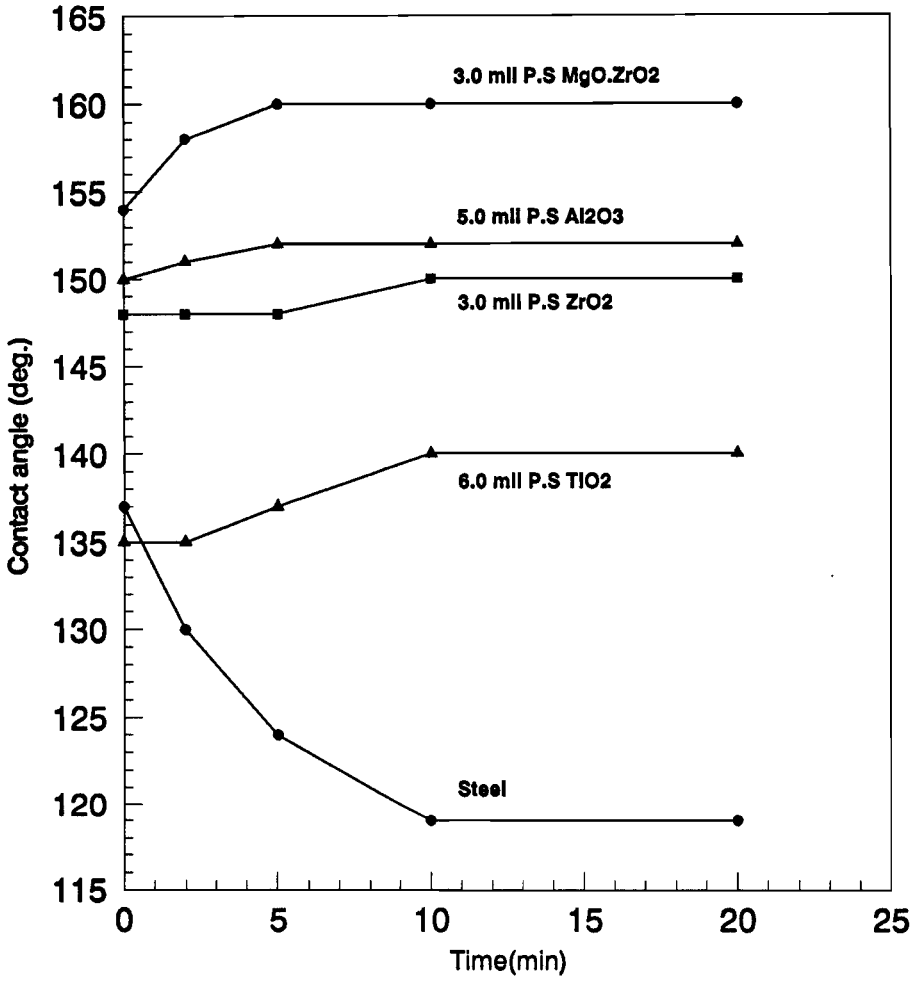

Figure (4.9) Contact angle versus time for aluminum 3105 on steel and coated substrates, (T=690°C).

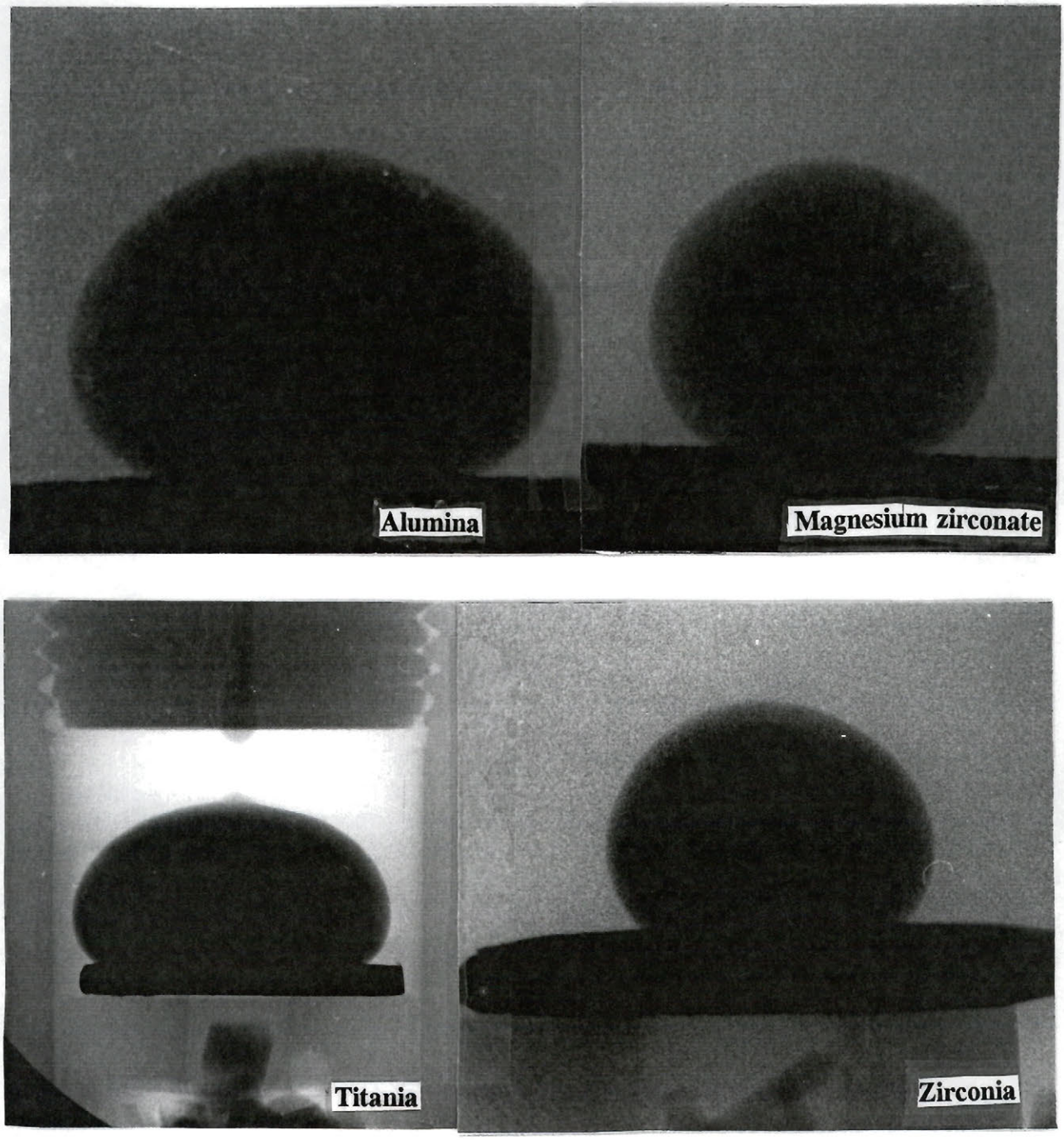

Figure (4.10) Photographs of Sessile Drops of Aluminum 3105 on Coated Substrates.

The experimental results, given in Figures (4.6) and (4.8), show a general trend in wettability of the two aluminum alloys on the various substrates investigated in this work : (a) both alloys wet the uncoated steel substrate more than any of the coating substrates, (b) among the four coated substrates, magnesium zirconate and titania show the least, and the most wettability , respectively, and (c) all coated substrates appear to be less wettable by aluminum alloy 3003 than they are by aluminum alloy 3105.

From the above mentioned Figures, it can also be seen that the wetting curves of both alloys, on all coated substrates, exhibit two areas of variation of θ with respect to time. The first area, typified by a positive slope; the contact angle increased with time up to about 5-10 minutes from the time the drop hit the substrate. In the second area, typified by a constant slope, the angle assumed its final equilibrium value and became time independent. The reason for the initial increase in contact angle may be attributed to :

(1) Gravity effect; as the drop hit the substrate, under the force of gravity, it spread widely on the substrate. As time progressed, the drop was allowed to rest on the solid substrate; and finally assuming its final contact angle.

(2) Oxygen effect; since the aluminum drop had to fall on the substrate, and was essentially stripped of its oxide layer, the surface of drop was, "relatively", free of oxygen during the initial minutes of contact. Although the system was highly evacuated, small amounts of oxygen still existed. Therefore, as time progressed, the drop surface contained more oxygen. The effect of oxygen was to increase the surface tension of the drop by forming an oxide layer, and consequently causing the contact angle to increase.

4.3.2.3 Analysis of Drop-Substrate Interface

After solidification, removing the aluminum drop from the steel substrate, was attempted. Drops of both alloys (AL-3003 and Al-3105) showed a strong adherence to the substrate; an indication that a reaction, at the interface, might have taken place. To confirm this, a spot analysis, using a back-scattered electron microscope, was carried out to determine the interface composition between a drop of aluminum 3105 and a steel substrate. As shown in Figure C2 of Appendix C, the interface consisted of about of 44 at% iron and 56 at% aluminum. Considering the Al-Fe phase diagram, (Figure B3, Appendix B), and applying the concept of the lever rule, it was found that the interface consisted of a mixture of Al_2Fe and AlFe.

On the contrary, aluminum drops solidified on all coating substrates showed no adherence; the drops were easily removed from the substrates, indicating that no reaction has taken place at the interface.

The microstructures of the bottom of the solidified Al-3003 drops were examined using the electron scanning microscopy. It can be seen from Figure (4.11) that a drop that solidified on magnesium zirconate, shows a large dendrite structure with a large dendrite spacing, which is a solidification characteristic of a free surface. Drops solidified on alumina, zirconia, and titania show a decrease in size of the dendrite structure in a descending order. The small dendrite structure is believed to be the result of a relatively good contact between the drop and the substrate; whereas poor contact (less wettability) results in a smaller dendrite structure. The microstructures of the solidified drops show a good agreement with the corresponding wettability curves given in Figure (4.7).

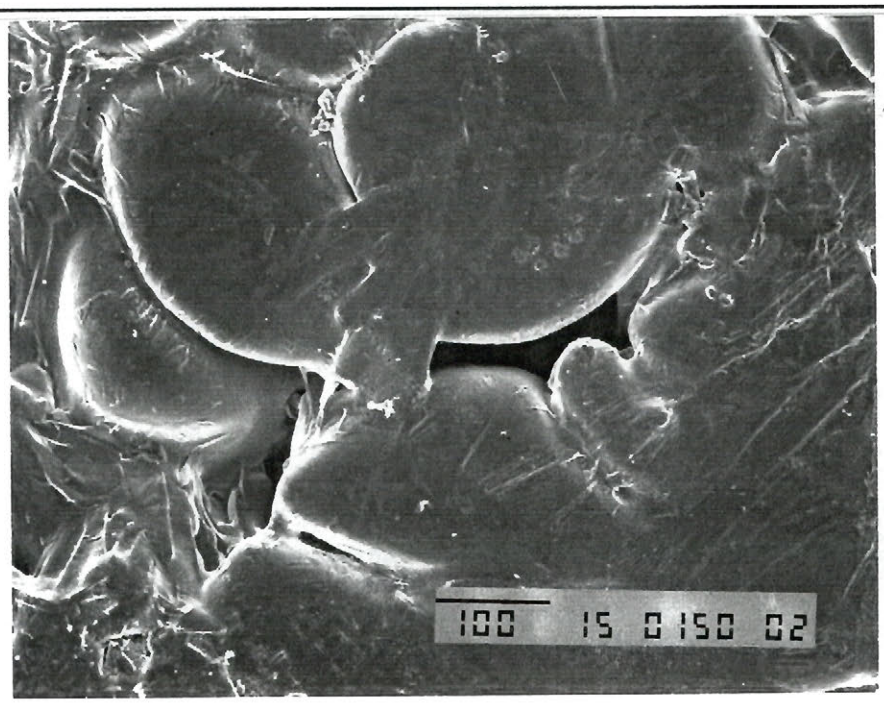

(a)

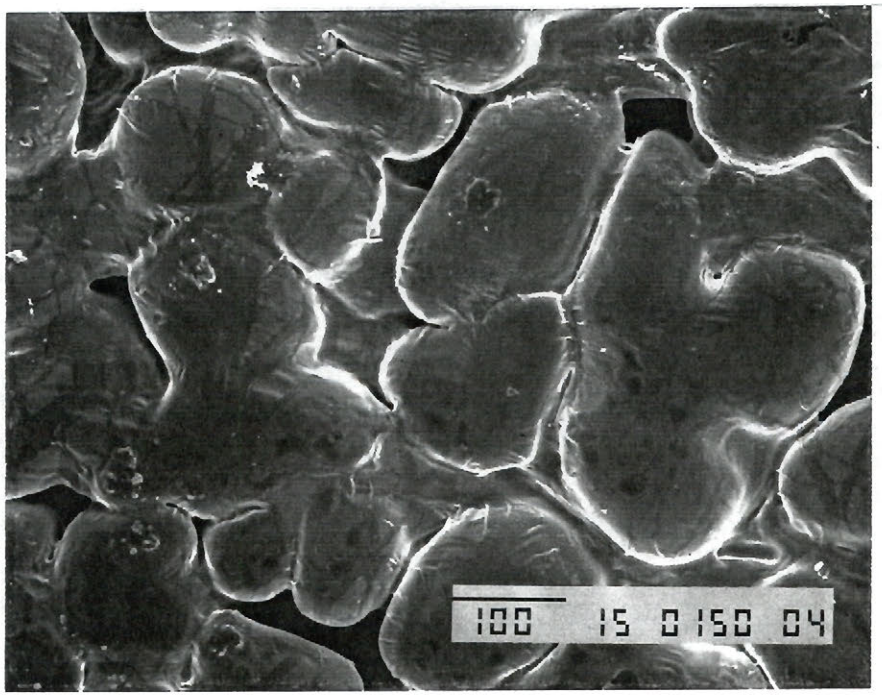

(b)

Figure (4.11) Scanning electron micrographs showing the bottom of a solidified aluminum 3003 drop on:
(a) Magnesium zirconate, (b) Alumina. ***(note the difference in the size of dendrites).***

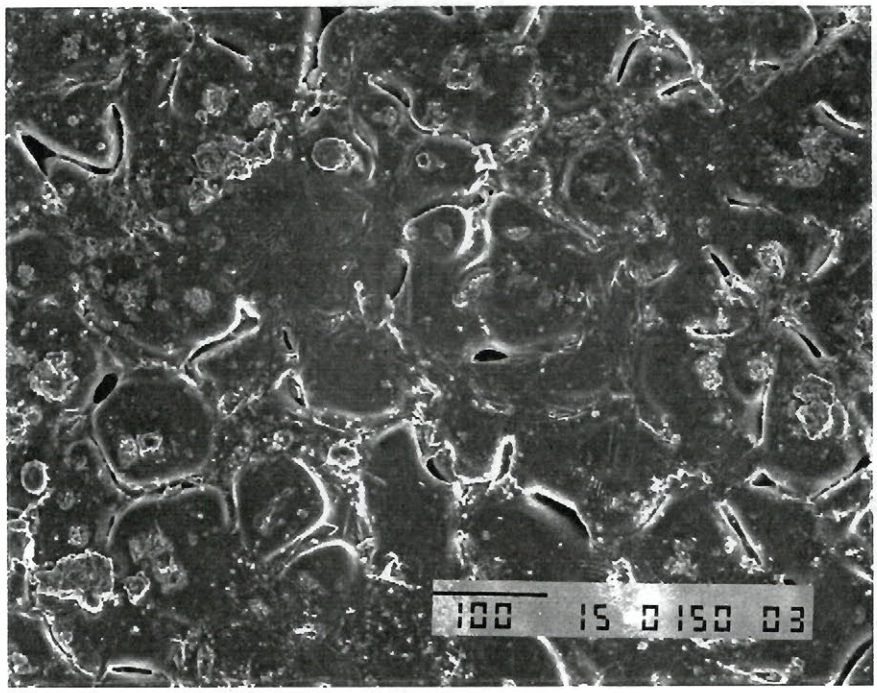

(c)

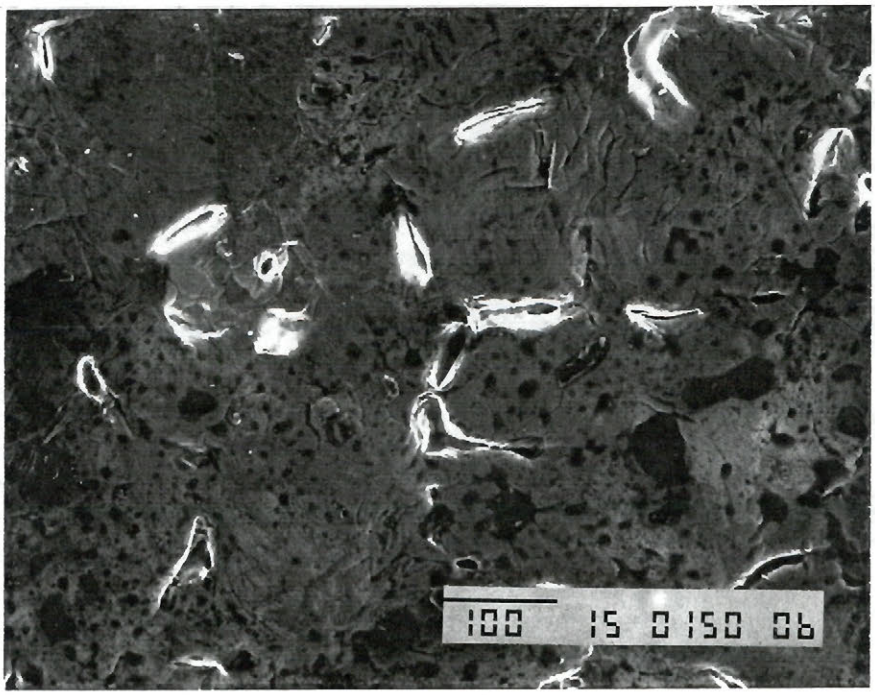

(d)

Figure (4.11) cont'd. (c) Zirconia, (d) Titania

CHAPTER
FIVE

CONCLUSIONS AND, SUGGESTIONS FOR FUTURE WORK

5.1 INTRODUCTION

In the past, static wettability studies have been carried out, largely, to study the formation of composites (i.e, on smooth substrates). Although, the effect of substrate roughness on wettability has been studied by several researchers, no data is available in the literature on the wettability of ceramic-coated substrates. This is the first time, to the author's knowledge, that a static wettability study has been carried out on plasma-coated ceramic substrates.

Traditionally, in forming composites, a substrate, that is highly wettable, is the most preferred. In our case, the situation was the opposite, i.e, the most preferred substrate was the one that exhibited less wettability. This is because, during continuous casting of a strip or slab, less wettability can lessen the friction between the casting and the substrate, and prevent sticking; therefore, allowing easy stripping of the cast. Furthermore, less wettability between the mould and the strand can result in a better surface quality of the cast product.

In this chapter, the conclusions to this wettability work are stated and suggestions, for future work, are outlined.

5.2 CONCLUSIONS

Since the degree of accuracy of measuring the wettability of most metals is greatly affected by the amount of oxygen present in the test chamber, and since the aluminum experiments were conducted in a better oxygen controlled conditions than those of the tin experiments, most of the concluding remarks, given below, are based on the aluminum experiments.

1 - At both 300°C and 690°C, the wettability of pure tin on a copper substrate is higher than that on a steel substrate.

2 - A 690°C, the wettability of aluminum alloys 3003 and 3105 on a steel (smooth surface) substrate is higher than that on all plasma-coated ceramic substrates (rough surfaces) that were investigated in this work.

3 - During the solidification of metals on uncoated substrates, reactions can occur at the metal-substrate interface, whereas no reactions occur during the solidification of metals on plasma-coated ceramic substrates.

4 - Carrying out static wettability experiments on plasma-coated ceramic substrates, under a controlled inert gas atmosphere, can give a good indication regarding the difference in wettability among these substrates.

5 - Of the four plasma-coated ceramic substrates studied in this work, magnesium zirconate ($MgO.ZrO_2$) and titania (TiO_2) showed the least, and the most, wettability, respectively.

6 - Alumina (Al_2O_3) and zirconia ($8\%Y_2O_3$-Zr_2O_3) showed less wettability than titania and more wettability than magnesium zirconate. Although no strong conclusion can be stated

regarding the difference in wettability between alumina and zirconia, most of our contact angle measurements showed that alumina was less wettable than zirconia.

5.3 SUGGESTED FUTURE WORK

In order to be able to answer many questions raised in this work regarding the selection of a certain type of ceramic material to serve as a coating for the casting steel belt, a wide variety of laboratory work is suggested. This includes;

1 - Ceramic coatings are applied to the steel belt either by plasma or flame spraying. In this work only the plasma-sprayed coatings were investigated. Therefore, it is suggested that similar experiments be conducted on the flame-sprayed ceramic coatings to study the difference in wettability, if any, between the plasma- and the flame-sprayed coatings.

2 - Experiments conducted to study the interaction of the material, used for the tip of the delivery nozzle, with different alloys in terms of fluidity, wettability, ... etc.

3 - Experiments conducted to study heat transfer through the different coatings using a variety of alloys.

4 - Investigate the effect of inert gas (such as N_2, He, Ar) on heat transfer through the coatings.

5 - Apply the laboratory findings to the industrial twin-belt caster.

REFERENCES

1. H. Tomono, W. Kurz, and W. Heinemann, **"The liquid steel meniscus in molds and its relevance to the surface quality of castings"**, *Metallurgical Transactions*, Vol. 12B, June 1981, pp. 409-413

2 - M. Wolf and W. Kurz, " **Solidification of steel in continuous-casting moulds"**, *Solidification and Casting of Metals, Proceeding of an International Conference held at the University of Sheffield* on 18-21 July 1977, pp. 287-294.

3 - A. Matsushita, K. Isogami, and M. Temma, **"Direct observation of molten steel meniscus in continuous casting mould during casting"**, *Transactions ISIJ*, Vol. 28, 1988, pp. 531-534.

4 - I. Saucedo, J. Beach and G. J. Davies, " **Heat Transfer and Solidification Kinetics in Meniscus Zone During Casting"**, *Metals Technology*, Vol. 9, July, 1982, pp. 282-290.

5 - J. Herbertson, P. C. Campbell, A. G. Hunt, and J. Freeman, **"Strip casting studies at BHP central research labaratories"**, *5th International Conference on Continuous Casting*, Linz, Voest Alpine, June 1990.

6 - R Alberny, " **Transfer de Chaleur et solidification en coulée continue"**, in *Coulée et Solidification de l'acier*, Luxembourg, November 29 to January 12, 1979.

7 - W. H. Emling and S. Dawson, **"Mould instrumentation for breakout detection and control"**, *Steelmaking Conference Proceedings*, Washington, DC, Vol. 74, 1991, pp. 197-217.

8 - James P. La Rue, **"Basic metal casting"**, *The American Foundarymen's Association*, p. 226.

9 - Peter C. Reagan, Jerome B. Allyn, and Takashi Okazaki, " **Hazelett twin-belt caster for thin slabs"**, *Iron and Steel Engineer*, February 1987, pp. 41-46.

10 - H. Bessemer, **"Ueber die Herstellung von endlosem Blech aus Schmiedbarem Eisen und stahl direct aus dem flüssigen metall"**, No. 11, 1891, pp. 921-926.

11 - R. William Hazelett, **"The present status of continuous casting between moving flexible belts"**, *Iron and Steel Engineer*, June 1966, pp. 105-110.

12 - H. Leon, **"Steel-Casting Programme - Justification Study"**, *A report prepared for the Canadian Workshop on Strip-Casting of Steel*, may 7-8, 1987, Hamilton, Ontario.

13 - I. V. Samarasekera and J. K. Brimacombe **"Heat extraction in the continuous casting of steel strip/thin slabs"**, *ibid.*

14 - S. Tanaka, **"Twin drum casting process for stainless steel strip"**, *The Korean Institute of Metals, SRNC-90*, pp. 643-652.

15 - Hazelett Strip-Casting Corporation, **"Twin-belt process for continuous casting"**, *Metallurgia*, Vol. 54, 1987, p. 189.

16 - Charles J. Petry, and Wojtek Szczypiorski, **"Update on continuous casting of aluminum alloys by the twin-belt process"**, *Light Metal Age*, August, 1986, pp. 19-25.

17 - C. J. Petry and S. W. Platek, **"Pogress report on the use of the Hazelett process for aluminum alloy strip-casting"**, *Light Metal Age*, 1983, pp. 931-950.

18 - Hazelett Strip-Casting Corporation, **"Continuous casting Twin-belt machine"**, *Metallurgia*, Vol. 53, 1986, p. 196.

19 - D. Reed von Gal, **"Twin-belt aluminum casting - A technology which has come of age"**, *Light Metal Age*, April, 1989, pp. 10-12, 35.

20 - Petry, C. J., **"Hazelett twin-belt caster"**, *Aluminum Association Continuous Casting Seminar, Kansas City*, October 1-2, 1975.

21 - C. J. Petry , S. W. Platek, and J. F. Wood, **"Expanding the Capabilities of the Hazelett Twin-BeltCaster : Mould Stabilization Techniques"**, *AIME*, February, 1982, pp. 851-872.

22 - I. V. Samarasekera and J. K. Brimacombe, **"Thermal field in continuous-casting moulds"**, *Canadian Metallurgical Quarterly*, Vol. 18, 1979, pp. 251-266.

23 - C. A. Miller, and E. Ruckenstein, **"The origin of flow during wetting of solids"**, *Journal of Colloid and Interface Science*, Vol. 48, No. 3, September 1974, pp. 368-381.

24 - J. Lopez, C. A. Miller, and E. Ruckenstein, **"Spreading kinetics of liquid drops on solids"**, *ibid*, Vol. 56, No. 3, September 1976, pp. 460-466.

25 - P. Nikolopoulos, G. Ondracek, and D. Sotiropoulou, **"Wettability and interfacial energies between zirconia ceramic and liquid metals"**, *Ceramics International*, Vol. 15, 1989, pp.201-206.

26 - R. D. Carnaham, T. L. Johnston, and C. H. Li, **"Some observations on the wetting of Al_2O_3 by aluminum"**, *Journal of The American Ceramic Society*, Vol. 41, 1958, pp. 343-347.

27 - T. Iida, and Roderick I. L. Guthrie, **"The physical properties of liquid metals"**, pp.109-115, 1988.

28 - M. Humenik, JR., and William D. Kingery, "**Metal-ceramic interaction: III, Surfaces tension and wettability of metal-ceramic systems**", *Ibid*, Vol. 37, No. 1, January, 1954, pp. 18-23.

29 - R. N. Wenzel, "**Surface roughness and contact angle**", *Industrial Engineering Chemistry*, Vol. 28, (1963), p. 988.

30 - R. H. Dettré and R. E. Johnson, " **Contact angle hysteresis**", *Advanced Chemcal Series*, No. 43, (1963), p. 136.

31 - R. E. Johnson and R. H. Dettré, "**The wettability and contact angle**", *Surface and Colloid Science*, Vol. 2, (1969), p. 107.

32 - S. J. Hitchcock, N. T. Carroll, and M. G. Nicholas, "**Some effects of substrate roughness on wettability**", *Journal of Materials Science*, Vol. 16, 1981, pp. 714-723.

33 - The United States Department of Energy, "**Thin section program**", *Cooperative Agreement No. DE-FCO7-84ID12545, Horizontal TSC Aprroach*, Vol. II, January, 1989.

34 - Greg Fisher, "**Ceramic coatings enhance performance engineering**", *Ceramic Bulletin*, Vol. 65 , No. 2, 1986, pp. 283-287.

35 - C. C. Nail and S. P. Situnayake, "**Refractory coatings for sand moulds**", *Foundry Trade Journal*, Vol. 12, March 1987, pp. 175-178.

36 - Thomas A. Taylor, Clifton G. Bergeron, and Richard A. Eppler, "**Ceramic Coating**", *Metals Handbook, Ninth Edition,, Surface Cleaning, Finishing,and Coating*, Vol. 5, 1982, pp. 532-547.

37 - Edward S. Hamel, **"Ceramic coatings: more than just wear resistant"**, *ME* ,August, 1986, pp. 30-34.

38 - Nippon Steel Technical Report No. 39, **"Ceramic coatings"**, January, 1989, pp. 41-43.

39 - Ke-shun Shi, Zeng-ying Qian, and, Ming-sie Zhuang, **"Microstructure and properties of sprayed ceramic coating"**, *Journal of Ceramic Society*, Vol. 71, 1988, pp. 924-929.

40 - D. Matejka and B. Benko, **"Plasma spraying of metallic and ceramic materials"**, 1989, pp. 47-52.

41 - R. Elsing, O. Knotek and, U. Balting, **"The influence of physical properties and spraying parameters on the creation of residual thermal stresses during the spraying process"**, *Surface and Coating Technology*, Vol. 41, 1990, pp. 147-156.

42 - E. Lugscheider, and T. Weber, **"Plasma spraying - an innovative coating technique: process variants and applications"**, *IEEE transactions on Plasma Science*, Vol. 18, No. 6, December, 1990, pp. 968-973.

43 - David L. Houck, **"Thermal spray : Advances in coating technology"**, *Proceedings of the national thermal spray conference*, 14-17 september, 1987, Orlando, Florida, U.S.A.

44 - F. Vasiliu, I. Pencela, Victor Manoliu, I. Dincă, and C. Sârbu, **"Thermal stability of plasma-sprayed zirconia coatings as related to substrate selection"**, *American Ceramic Society Bulletin*, Vol. 64, 1985, pp. 1268-1271.

45 - R. M. Burns, and W. W. Bradley, **"Protective coatings for metals"**, Third eddition, No. 163, 1967, pp.

46 - Yehuda Rotenberg, **"The program Axisymmetric Drop Shape Analysis - Profile (ADSAP)"**, *Department of Mechanical Engineering, University of Toronto*, July, 1988.

47 - Scott K. T., **"Plasma-Sprayed Ceramic Coatings"**, in *British Ceraimc Proceerings, Ceramic Surfaces and Surface Treatments*, No. 34, august, 1984, pp. 195-205.

48 - **"Selected values of the thermodynamic properties of binary alloys"**, Published by *American Society for Metals*, 1973, pp. 797, 886, and 158.

APPENDICES

APPENDIX A.

SAMPLE: Al 3003 on ZrO_2, (T=690°C), Time = 2 min.

Input Data

980.4 2.710000 0.496334 42 1 500 1
0.512862 0.482471
0.340775 0.000000
0.294175 0.003615
0.258247 0.000198
0.229718 0.005276
0.187719 0.018970
0.149775 0.032213
0.116511 0.052413
0.084474 0.082386
0.056059 0.117449
0.037842 0.140948
0.018896 0.178160
0.009044 0.214901
0.004551 0.257843
0.000000 0.295029
0.006570 0.347714
0.015947 0.385138
0.033254 0.413514
0.056365 0.442788
0.070155 0.458869
0.085612 0.470064
0.540098 0.457066
0.561929 0.433860
0.578161 0.404466
0.593168 0.379215
0.602604 0.343695
0.608475 0.308840
0.609857 0.266060
0.605089 0.243513
0.594288 0.206403
0.587231 0.181335
0.575272 0.158921
0.557253 0.139940
0.543156 0.113318
0.528260 0.094415
0.513410 0.081029

Computational Results

A. Origin of the drop coordinate system
X0 (cm) ..... 0.302585D+00
Z0 (cm).....-0.353571D-03
B. Radius of curvature at origin (cm).....0.319282D+00
C. Surface tension (ergs/cm sq.).....0.873639D+03
D. Surface area (cm sq.) .....0.984745D+00
E. Volume (cm cu.) .....0.104599D+00
F. Contact angle (degrees) .....0.155243D+03
G. Contact radius (cm) .....0.180058D+00

APPENDIX A.

Table 1A. Contact angle vs. time for tin on various substrates, (T = 300°C).

	Contact angle (deg.)					
Substrate	$MgO.ZrO_2$	Al_2O_3	ZrO_2	TiO_2	Steel	Copper
Time (min.)						
2	165	163	163	160	150	112
5	165	163	163	160	148	112
8	164	163	163	160	148	107
12	162	160	163	158	148	104
15	162	160	163	158	146	98
20	162	160	163	158	146	98

Table 2A. Contact angle vs. time for tin, (T = 690°C)

	Contact angle (deg.)					
Substrate	$MgO.ZrO_2$	Al_2O_3	ZrO_2	TiO_2	Steel	Copper
Time (min.)						
2	155	151	150	142	135	90
5	155	150	150	142	130	78
8	153	148	145	140	124	67
12	153	148	145	138	120	49
15	153	148	145	138	112	32
20	153	148	145	138	112	32

Table 3A. Contact angle vs. time for Al 3003, (T = 690°C).

	Contact angle (deg.).				
Substrate	$MgO.ZrO_2$	ZrO_2	Al_2O_3	TiO_2	Steel
Time (min.)					
0	165	155	160	143	135
2	166	155	160	143	129
5	168	156	162	144	125
10	168	156	162	144	115
20	168	156	162	144	115

Table 4A. Contact angle vs. Time for Al 3105, (T = 690°C).

	Contact angle (deg.)				
Substrate	$MgO.ZrO_2$	ZrO_2	Al_2O_3	TiO_2	Steel
Time (min.)					
0	154	148	150	135	137
2	158	148	151	135	130
5	160	148	152	137	124
10	160	150	152	140	119
20	160	150	152	140	119

APPENDIX B.

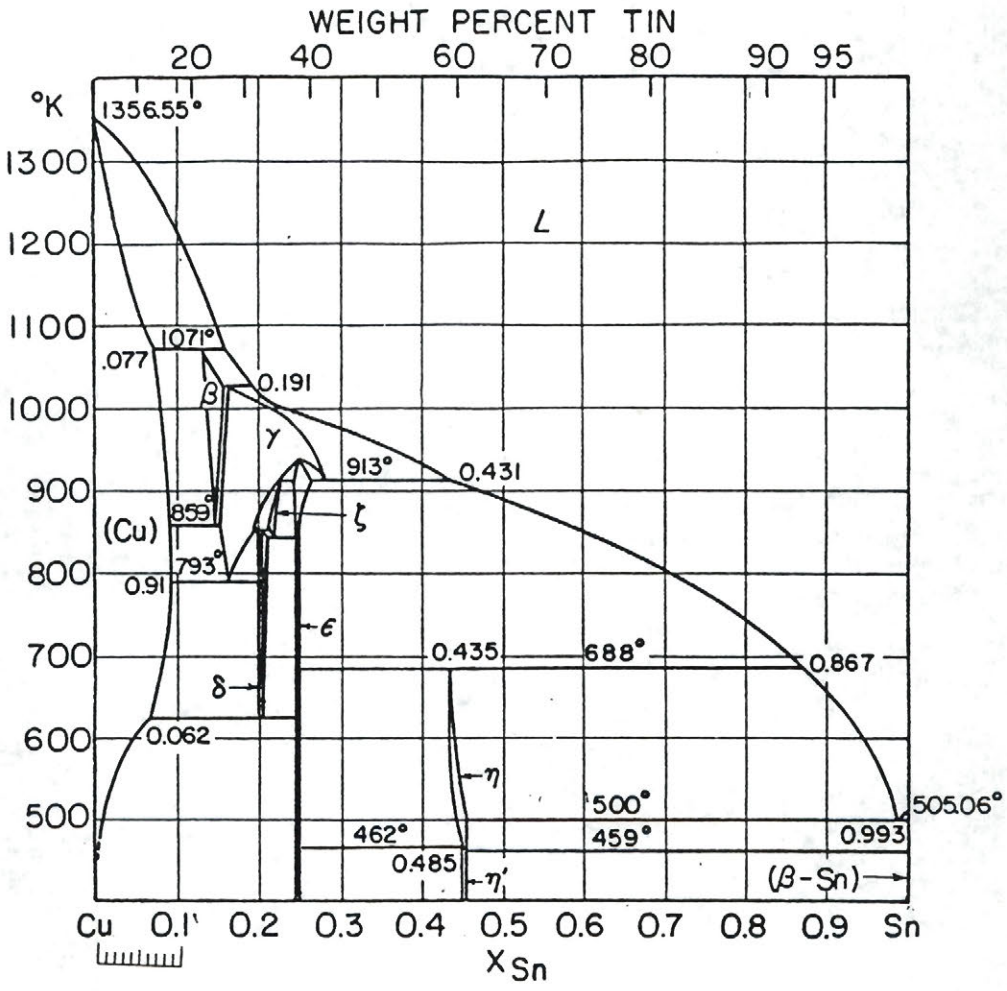

Figure 1B. Tin-Copper-Phase Equilibrium Diagram[48].

($\delta = Cu_{31}Sn_8$, $\zeta = Cu_{20}Sn_6$, $\epsilon = Cu_3Sn$, $\eta = Cu_6Sn_5$).

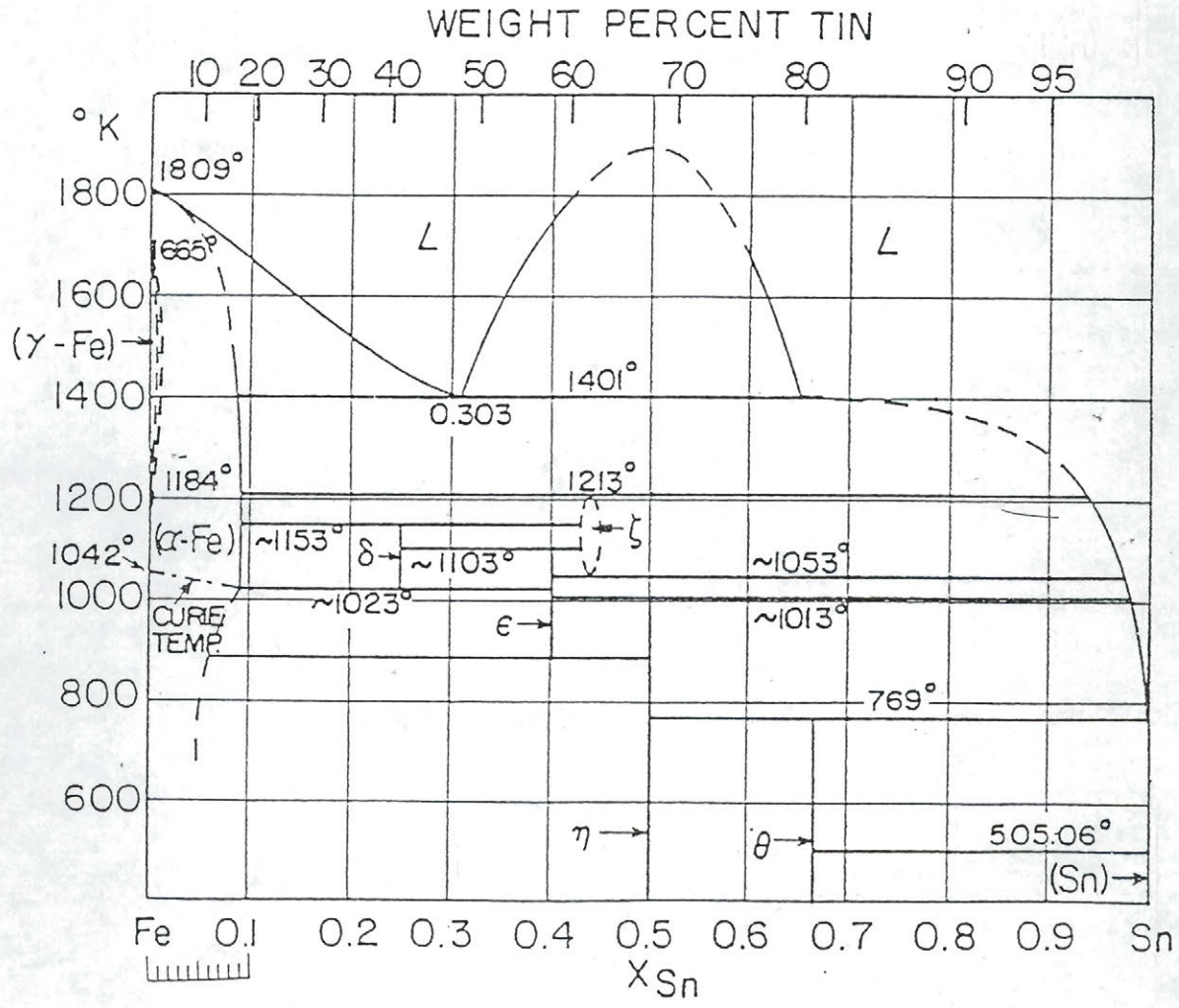

Figure 2B. Tin-Iron Equilibrium Phase Diagram[48].

(δ = Fe_3Sn_2, ϵ = Fe_3Sn, ζ = $Fe_{1.3}Sn$, η = FeSn, θ = $FeSn_2$).

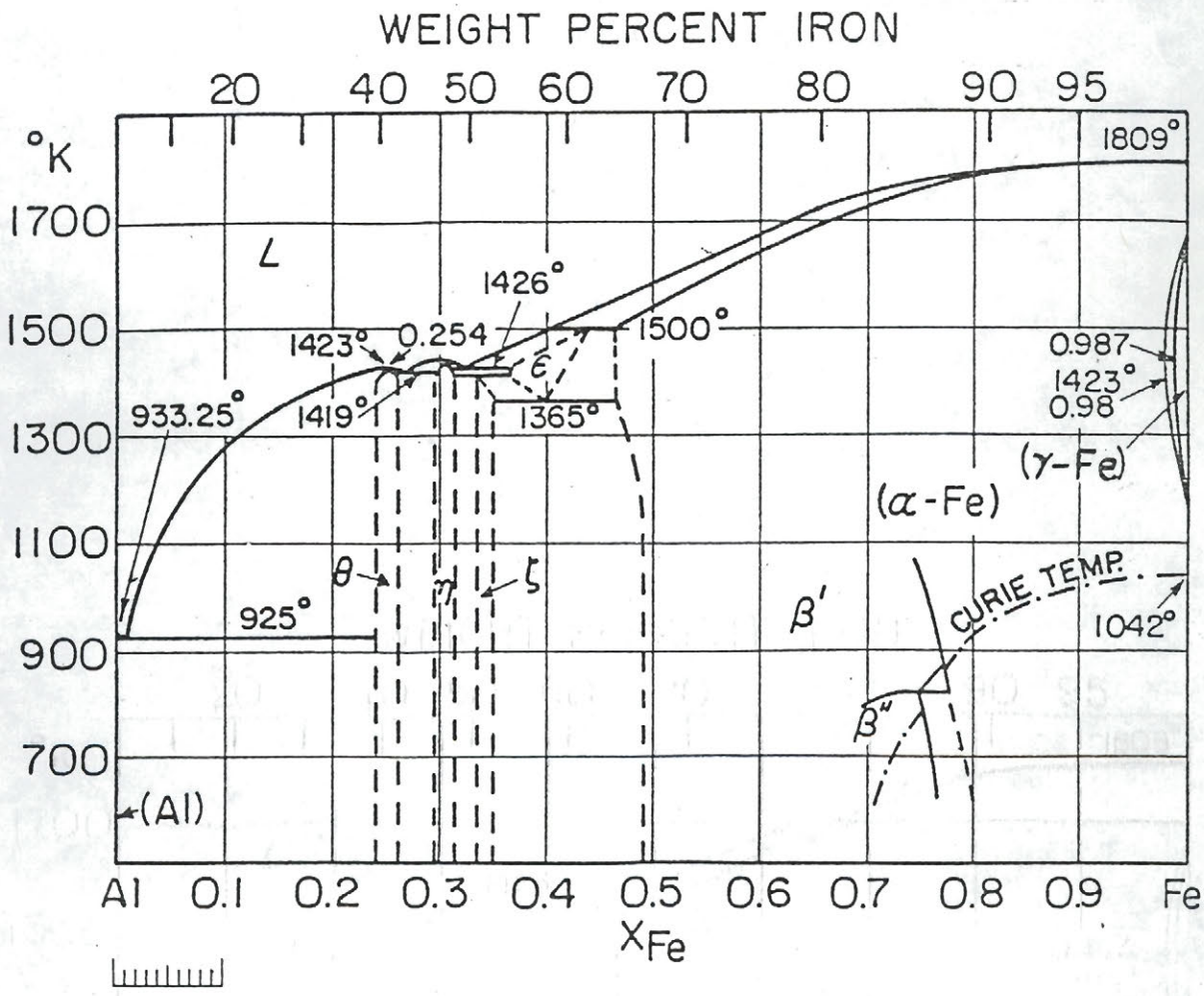

Figure 3B. Aluminum-Iron Equilibrium Phase Diagram[48].

(θ = Al_3Fe, η = Al_5Fe_2, β' = AlFe, β'' = $AlFe_3$, ζ = Al_2Fe).

APPENDIX C.

Element	K-ratio	Z	A	F	ZAF	Atom%	Wt%
Cu-K	0.605	0.954	1.030	1.000	0.982	73.23	59.42
Sn-L	0.370	1.070	1.030	0.995	1.096	26.77	40.58
						Total=	100.00%

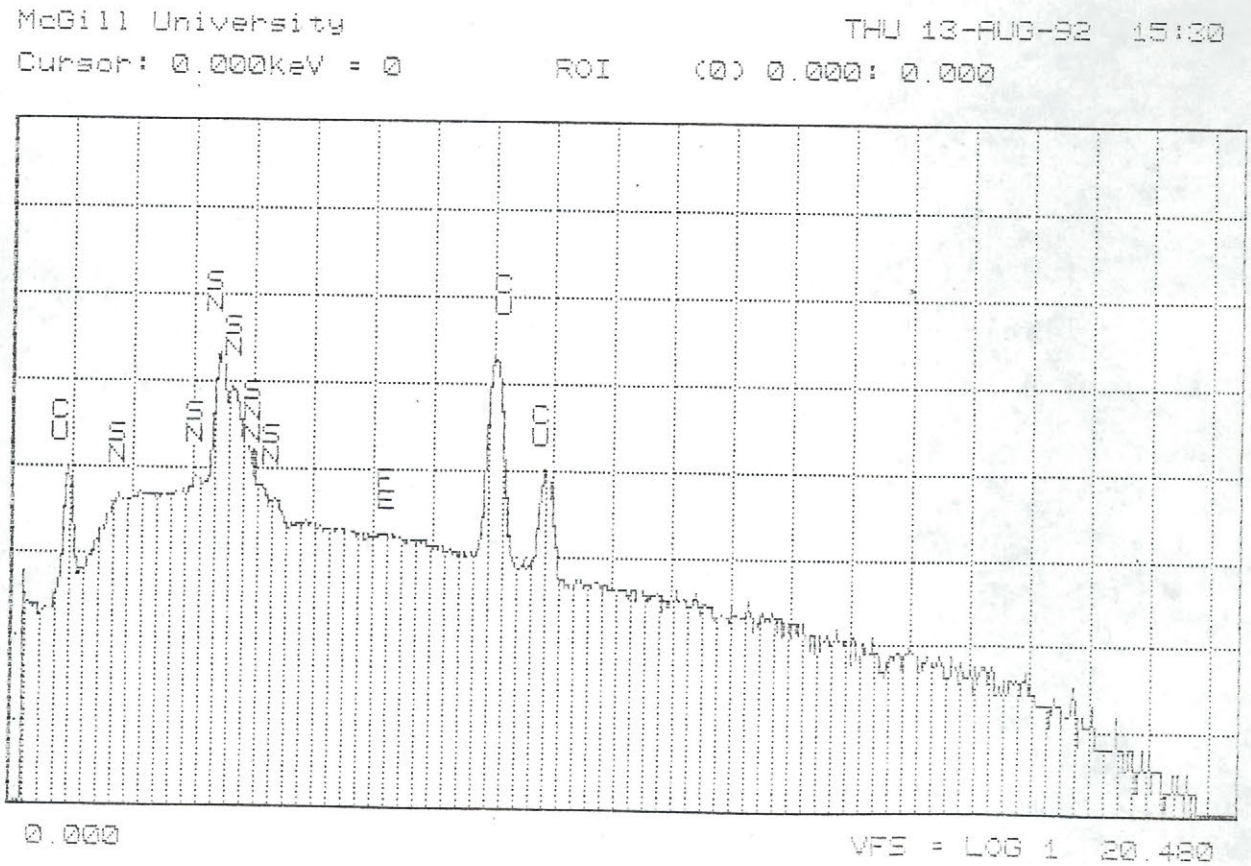

(a) Dark area.

Figure 1C Composition of Sn-Cu interface.

Element	K-ratio	Z	A	F	ZAF	Atom%	Wt%
Cu-K	0.314	0.918	1.052	1.000	0.966	44.84	30.33
Sn-L	0.663	1.037	1.015	0.998	1.050	55.16	69.67
						Total=	100.00%

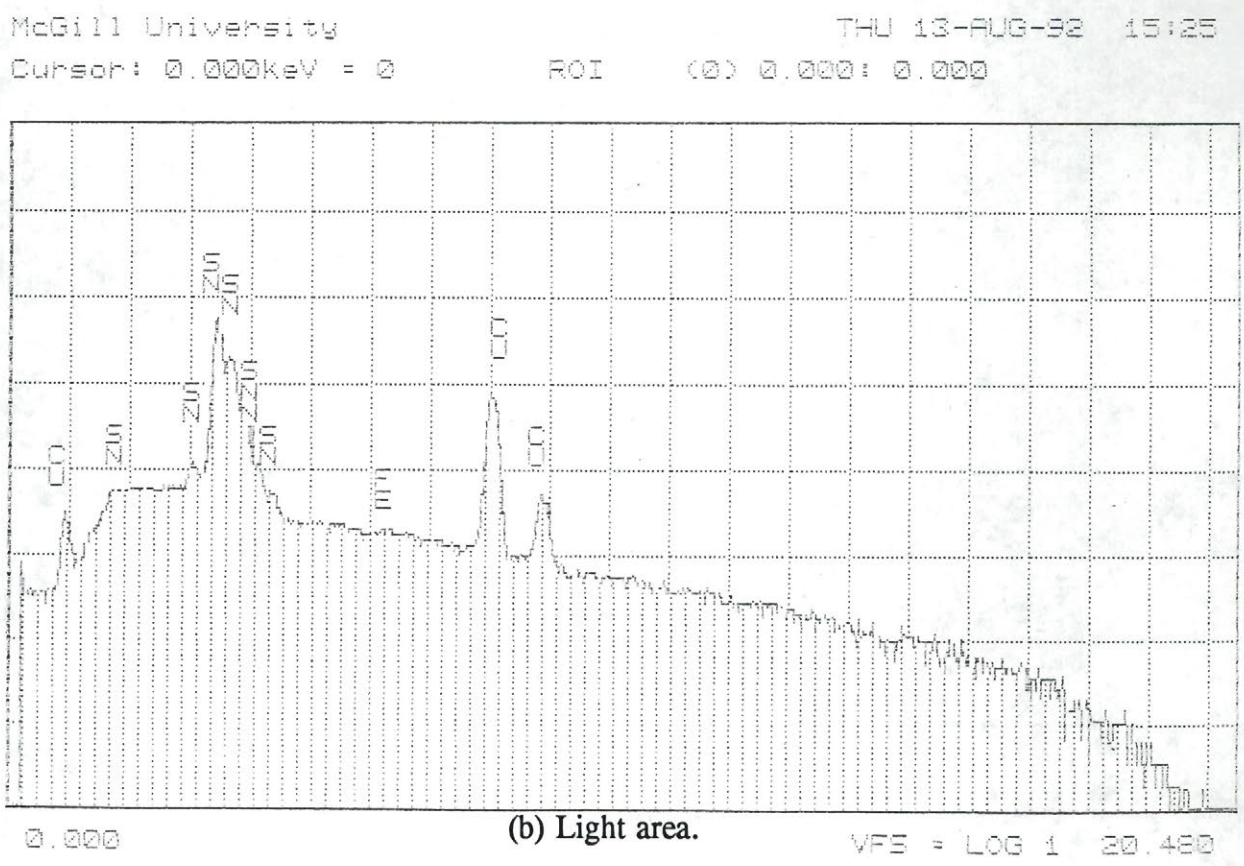

(b) Light area.

Figure C1. Cont,d.

Element	K-ratio	Z	A	F	ZAF	Atom%	Wt%
Fe	0.592	1.037	1.005	1.000	1.043	43.74	61.67
Al	0.201	0.961	1.983	1.000	1.904	56.26	38.33
						Total=	100.00%

SQ: SETUP DEFINITIONS

McGill University WED 19-AUG-92 14:51
Cursor: 0.000keV = 0

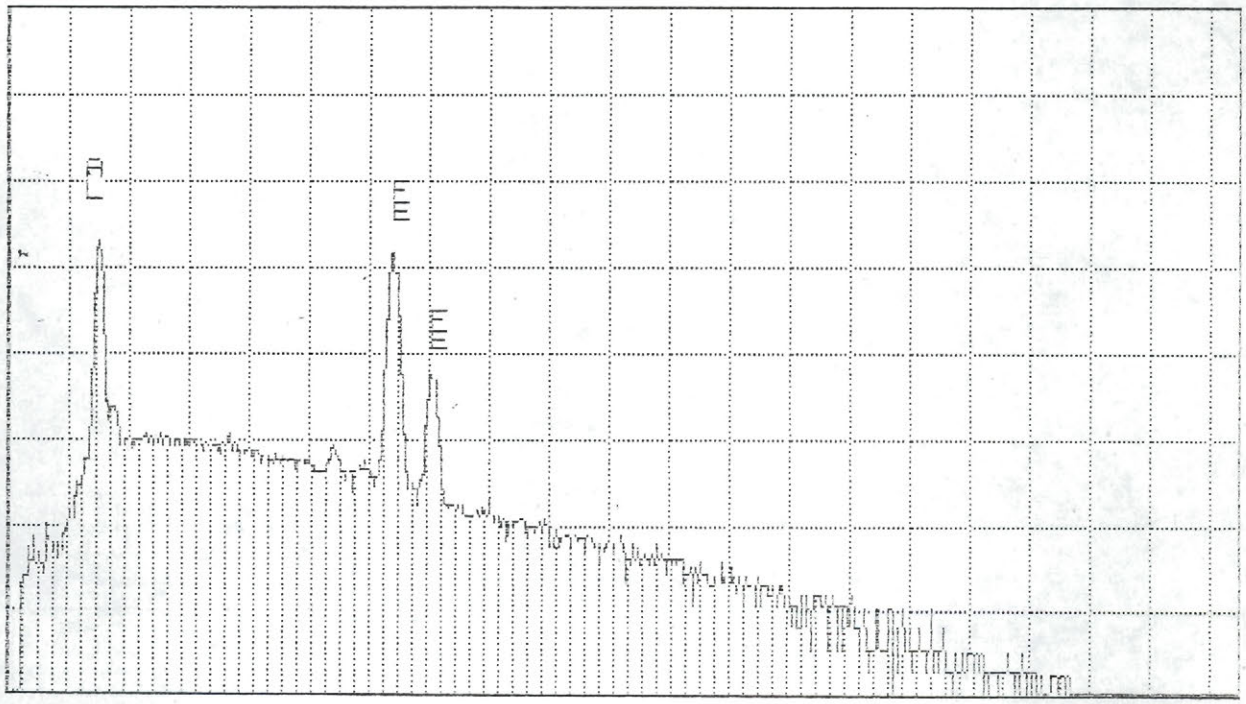

0.000 VFS = LOG 1 20.480

Figure 2C Composition of Al-Fe Interface.